Geochronology of faults

	MIURA Kazumasa
journal or publication title	Full
	13301　2145
	2023-03-22
URL	http://hdl.handle.net/2297/00069932

博　士　論　文

Geochronology of faults

金沢大学大学院自然科学研究科

氏　　名　　三浦　知督

提出年月　　2023 年 1 月 6 日

TABLE OF CONTENTS

LIST OF FIGURES

Chapter 4

LIST OF TABLE

ACKOWNLEGMENTS

ABSTRACT

Japan is one of the most earthquake-prone regions in the world. Numerous attempts have been made to determine the age of fault activity recorded in fault rocks using dating methods such as K-Ar, fission track, electron spin resonance and luminescence dating methods. Compared to other methods, the signal reset occurs in very short time even at low temperatures in luminescence dating, and it has a potential to identify the time of final activity of faulting, for the faulting should cause the frictional heating and result in erasing accumulated luminescence signals. Therefore, this study attempted to elucidate the influence of fault activity on the luminescence signal using quartz samples collected from the Nojima active fault. First we analysed the thermoluminescence (TL) signals and estimated signal decrease according to the distance from the fault. Second, we investigated how the optically stimulated luminescence (OSL) signal in quartz decrease by the faulting through friction experiments to determine the seismological and geological conditions necessary for the resetting of the OSL signal in natural fault zones.

The Nojima Fault is extending from north-east to south-west of Awaji Island in south-west Japan and caused the 1995 Hyogo-ken Nanbu Earthquake (M = 7.3) at 5:46 a.m. on January 17, 1995. A clear surface displacement was discovered along the Nojima Fault. The trench survey was conducted at a locality 720 m east-southeast of the Hokudan Earthquake Memorial Park in Ogura, Awaji City, with a dimension of 15 m long in a northwest–southeast direction, 2.5–5 m wide, and 1.5–3 m deep.

Samples were taken from the south wall of the trench. One sample was collected from the gouge and seven samples were collected from the granite breccias zone at 1 m intervals to the east of the gouge; S7 was collected from only a few millimeters away from the gouge sample. In addition, one sample was collected from the east wall, which is the furthest from the fault in the trench (E1). All of these samples were affected to some extent by fault activity. Two granite samples were also collected from the subsurface, which were less affected by fault activity. One was taken from a point approximately 200 m east of the trench (base rock [BR]) and the other from a point approximately 3 km from the fault in the Tsushigawa Granite (TS).

The examination of luminescence-emitting temperatures revealed that quartz separated from granite has four luminescence sites (roughly the peak temperatures of 200°C, 270°C, 340°C, and 400°C under a heating rate of 1°C/s). The lifetime of each luminescence site was then estimated. Accumulated doses and ages were determined for each luminescence site under the annual doses estimated from the radioisotope concentrations of samples, which were measured by XRF and ICP-MS.

Two basement samples showed concordant ages of 40 ka at 270°C and 340°C emissions and more than 80 ka at a 400°C emission. These ages may be representative of the uplifting process of the basement granite. Two samples collected near the fault showed young ages compared with those of

the other samples, but they were not consistent with the time of the last fault activity (about 30 years ago) partly because TL is not capable of dating modern events. The other trench samples showed various ages at 270°C and 340°C emissions different from that of the basement granite, indicating that the fault activity had some effects on the signal.

In the frictional experiments, we used quartz sand separated from the basement granite with a particle size of <150 μm and equivalent dose of 31.5 ± 16.6 Gy, given artificially by gamma ray irradiation. Friction experiments were conducted in Yamaguchi University with a rotary-shear, high-velocity friction apparatus at slip rates (V) of 200 μm s^{-1} to 1.3 m s^{-1}, normal stress of 1.0 MPa, and displacement of 10 m.

In the experiments conducted under dry conditions, the OSL signal starts to decrease from $V =$ 0.25 m s^{-1} and becomes near zero at $V \geq 0.65$ ms^{-1}. OSL signal resetting is also observed in the experiment sheared at 1.3 ms^{-1} under water-added conditions. At $V = 0.25$ and 0.40 ms^{-1}, partial resetting occurs, which is characterized by coexistence of particles with and without an OSL signal.

OSL signal intensity shows a strong correlation with applied power density and frictional heat during high-velocity friction, and the signal exponentially decreases with increasing power density and temperature. The power density required for partial and complete OSL signal resetting is ~0.17 and 0.6 MW m^{-2}, respectively. Assuming a co-seismic fault slip rate of 0.6 m s^{-1}, the depths required for partial and complete resetting are expected to be ≥11 and ≥42 m.

Based on these results, it is currently difficult to identify the timing of the last activity using a sample collected from the surface fault gouge. However, with future improvements in sampling methods and measurement precision and accuracy, with the use of a larger number of samples, and with the possibility of collecting fault samples from deeper seismic intensities, it may be possible to identify the timing of the final activity period.

CHAPTER 1

1. Introduction

1.1 Past disasters caused by the fault activity

Japan is one of the most earthquake-prone regions in the world. There are more than 1,000 active faults in the Japanese archipelago. The degree of activity varies widely, with recurrence intervals ranging from thousands to tens of thousands of years(Yamazaki, 1998).Some of these faults have caused extensive damage in the past. The recent earthquakes which gave significant damage to the society are shown on the map (Figure. 1-1).

The 2011 off the Pacific coast of Tohoku Earthquake (M = 9.0)occurred along the subduction zone, the boundary between the Pacific and North American plates, and the displacement is estimated to have reached 65 m (Sun et al., 2016). The earthquake generated an enormous tsunami, which reached a height of 8-9 m (Japan Weather Association, 2011), resulting in more than 20 000 people dead or missing and more than 400,000 buildings destroyed (Fire and Disaster Management Agency, 2022).

The Mid Niigata Prefecture Earthquake in 2004 (M = 6.8) was initially believed to be caused by the Obiro Fault and the northern segment of the western boundary fault of the Muikamachi Basin(Suzuki et al., 2006). However, other studies have suggested that it was caused by an unknown reverse fault under a northwest-southeast compressive stress field in the vicinity of the above faults (Hikima et al. 2005).The earthquake caused 68 deaths. This disaster is also known for the derailing of the Joetsu Shinkansen bullet train (Fire and Disaster Management Agency, 2009). A lot of collapses of roads and landsliding were reported (Mori et al., 2005).

Furthermore, the 2016 Kumamoto Earthquake (M = 6.4, M = 7.3) in April 2016 killed more than 200 people. More than 8,000 houses collapsed (Aoki, 2017). The M6.4 earthquake on 14th April occurred on the Hinagu fault and the M 7.3 earthquake on 16th April occurred along the Futagawa fault (Goda et al., 2016, Kato et al., 2016).

One of recent earthquakes that is still fresh in the memory is the 2018 Hokkaido Eastern Iburi earthquake (M = 6.7) occurred in September 2018. The epicenter of this earthquake locates on a reverse fault formed under a northeast-east-west-southwest compressive stress field (Gou et al., 2019). The earthquake caused 43 fatalities and the largest landslide since the Meiji Era (Murakami et al., 2020).

The northern Noto Peninsula in Ishikawa Prefecture has also attracted attention in recent years because of frequent earthquakes. A southeast-trending reverse fault is known in this area and caused the 2007 earthquake (Hiramatsu, 2007). It has been suggested that fluids in the lower Noto Peninsula may have been involved in these earthquakes. Stress changes caused by this unsteady crustal deformation may have affected existing active faults in the northern Noto Peninsula (Hiramatsu, 2022).

The 1995 Hyogo-ken Nanbu earthquake (M = 7.3) had its hypoentre on the Nojima fault in the

north-east of Awaji Island, and is the research target of this paper. The earthquake caused more than 6,000 deaths (Fire and Disaster Management Agency, 2006).

1.2 Previous attempt to date fault activity

As mentioned in 1.1, there are many earthquakes caused by the active faults, and these seismological activities have a certain periodicity. Therefore, identifying the last activity along faults and revealing the recurrence interval in earthquakes caused by their activity is important for earthquake prediction, that is necessary to prepare for disasters. Activity of faults in the observational period has been easily identified and examined. Several historical earthquakes have been attributed to the same active fault, or the same fault has been attributed to several historical earthquakes (Odagiri et al., 2001).Some large scale earthquakes are recorded in the historical literatures, but it is difficult to attribute them to particular active faultings. Moreover, there are probably many earthquakes not mentioned in the literature, so that revealing the last faulting and recurrence interval is even more difficult. This concept has led to various approaches to the dating of active faults.

Numerous attempts have been made to determine the age of fault activity recorded in fault rocks using dating methods such as K-Ar, fission track(FT), electron spin resonance(ESR) and luminescence dating methods.

The K-Ar dating method was successfully applied to the faults worldwide. The recent research includes dating of fault gouges in Western Norway (Hestnes et al., 2022), geological faults in the Central Alps (Pleuger et al., 2012) and the Nojima Fault, Japan (Zwingmann et al., 2010).Dating of active faults using the K-Ar method analyses clay minerals produced by hydrothermal activity within the fault(Lyons and Snellenburg,1971). However, fractured products can also be mixed with the clay minerals resulting from fault activity and original minerals included in the host rock (Tamura et al., 2013). Therefore, the measurement are often applied to samples with several grain sizes. The reason for this is to estimate degree of contamination of residual K-containing minerals such as K-feldspar and mica. Therefore, different ages tend to be calculated for the same sample depending on the grain size (Zwingmann et al., 2010).

A number of FT applications has also been published, including a study targeting the Nojima fault (Yamada et al., 2007), the Atotsugawa fault (Sueoka et al., 2019) and the Elbe fault in Germany (Käßner et al., 2020).

The above two dating methods are applicable to geological time period due to their relatively longer half lives: the FT method is mainly used for dating older than 10,000 years (Muramatsu, 1987). The K-Ar method has a confidence dating limit of tens of thousands of years, butfor volcanic rocks, dating of rocks younger than 10,000 years has been tried (Itaya et al., 1995). From this point of view, these methods are not very suitable for identifying the time of the last faulting activity.

Furthermore, a number of studies have also been published on ESR methods, including studies

investigating faults in China (Qiu et al., 2018), the Wangsan fault in Korea (Lee et al., 2003) and the Nojima fault (Fukuchi, 2001).

Compared to these methods, the signal reset occurs in very short time even at low temperatures in luminescence dating, and it has a potential to identify the time of final activity of faulting, for the faulting should cause the frictional heating and result in erasing accumulated luminescence signals. Luminescence dating was applied to the Atotsugawa Fault (Ganzawa et al., 2013), the San Andreas Fault (Spencer et al., 2012), and the Sabzevar fault in north-east Iran (Fattahi et al., 2006).In case of luminescence dating, the understanding how faulting (especially the deformation of minerals) affects the luminescence dating system is still ongoing.

This study attempted to elucidate the influence of fault activity on the luminescence signal using quartz samples collected from the Nojima active faults. First we analysed the thermoluminescence (TL) signals and estimated signal decrease according to the distance from the fault. The result is shown in chapter 2. Second, we investigated how the optically stimulated luminescence (OSL) signal in quartz decrease by the faulting through friction experiments to determine the seismological and geological conditions necessary for the resetting of the OSL signal in natural fault zones. The result is shown in chapter 3. Chapter 4 demonstrate.
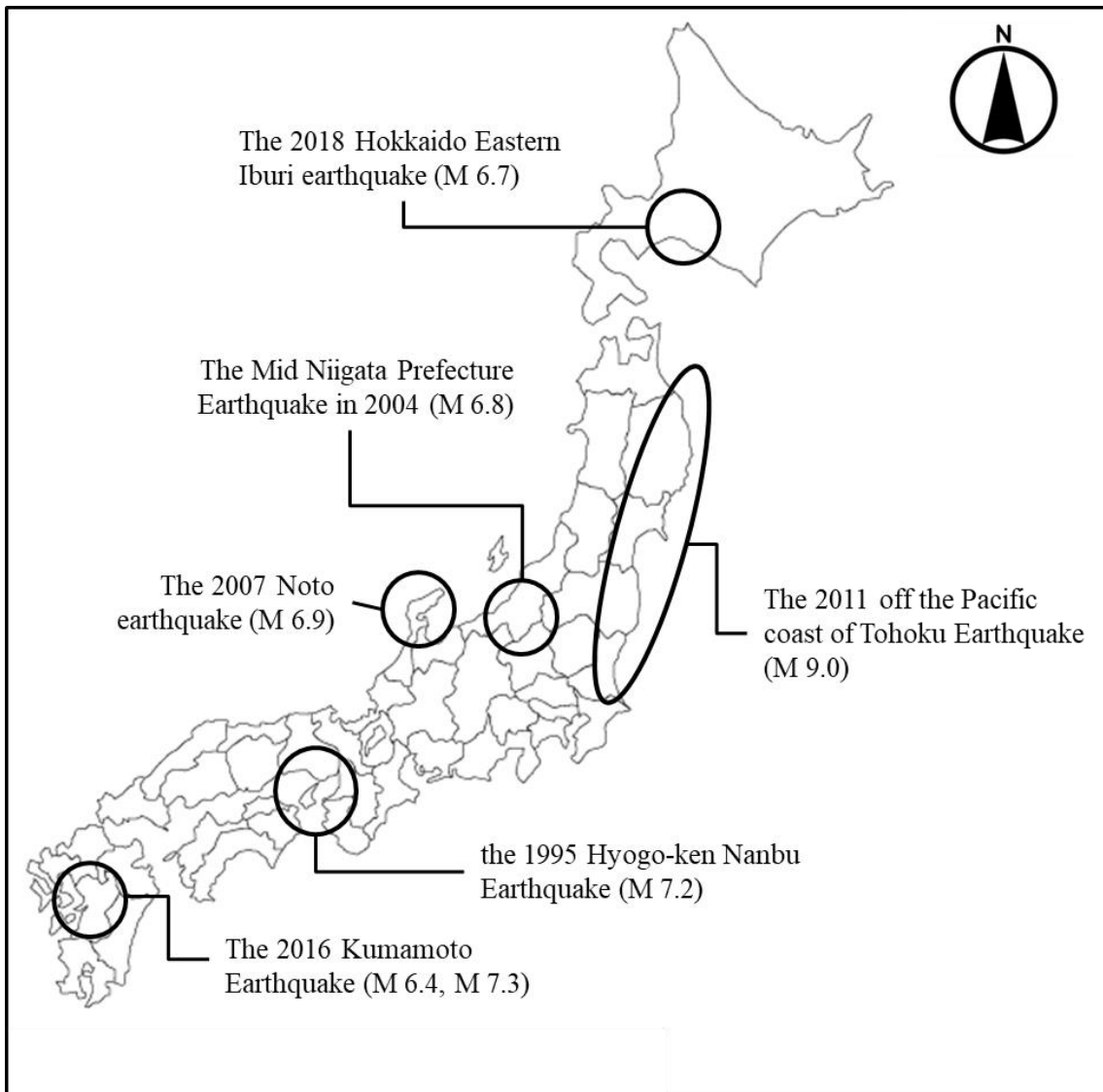
Figure 1-1. Examples of earthquakes that have caused significant damage in Japan in the recent past. The location of the circle is a rough earthquake damage area; the size of the circle does not indicate the magnitude of the earthquake.

1.3 Reference

Aoki H. (2017) Overview of the 2016 Kumamoto earthquake, Disaster information, No.15-2 , https://doi.org/10.24709/jasdis.15.2_77 (in Japanese)

Fattahi M. Walher R. Hollingsworth J. Bahroudi A. Nazari H. Talebian M. Armitage A. and Stokes S. (2006) Holocene slip-rate on the Sabzevar thrust fault, NE Iran, determined using optically stimulated luminescence (OSL), Earth and Planetary Science Letters, Vol. 245, Issues 3-4, pages 673-684,https://doi.org/10.1016/j.epsl.2006.03.027

Fire and Disaster Management Agency (2006) Document 3-1-1: Overview of the Great Hanshin-Awaji Earthquake, The Great Hanshin-Awaji Earthquake (Final Report) (in Japanese)

Fire and Disaster Management Agency (2009) 2004 Niigata-Chuetsu Earthquake (Definitive Report) (in Japanese)

Fire and Disaster Management Agency (2022) 2011 Tohoku-Pacific Ocean Earthquake (Great East Japan Earthquake) (Report No. 162) (in Japanese)

Fukuchi T. (2001) Assessment of fault activity by ESR dating of fault gouge; an example of the 500 m core samples drilled into the Nojima earthquake fault in Japan, Quaternary Science Reviews, Vol. 20, Issues 5-9, pages 1005-1008, https://doi.org/10.1016/S0277-3791(00)00064-0

Ganzawa Y. Takahashi C. Miura K. and Shimizu S. (2013) Dating of active fault gouge using optical stimulated luminescence and thermoluminescence, The Journal of the Geological Society of Japan, 119, 714-726

Goda K. Campbell G. Hulme L. Ismael B. Ke L. Marsh R. Sammond P. So E. Okumura Y. Kishi N. Koyama M. Yotsui S. Kiyono J. Wu S. and Wilkinson S. (2016) The 2016 Kumamoto earthquakes:cascading geological hazards andcompounding risks, Frontiers in Built Environment,Vol. 2, Article 19, pages 1-23, DOI: 10.3389/fbuil.2016.00019

Gou T. Huang Z. Zhao D. and Wang L. (2019) Structural Heterogeneity and Anisotropy in the Source Zone of the 2018 Eastern Iburi Earthquake in Hokkaido, Japan, Journal of Geophysical Research, 124,7052–7066. DOI: 10.1029/2019JB017388

Heatnes Å. Gasser D. Scheiber T. Jacobs J. Lelij R. Schönenberger J. and Ksienzyk A (2022) The brittle evolution of Western Norway – A space-time model based on fault mineralizations, K–Ar fault gouge dating and paleostress analysis, Journal of Structural Geology,160, https://doi.org/10.1016/j.jsg.2022.104621

Hikima K. and Koketsu K. (2005) Rupture processes of the 2004 Chuetsu (mid-Niigata prefecture) earthquake, Japan: A series of events in a complex fault system, Geophysical Research Letters, Volume 32, Issue 18, 03, DOI: 10.1029/2005GL023588

Hiramatsu Y. (2007) The Noto Hanto earthquake in 2007 : Seismicityand Mechanism, EarthSciencc, Vol. 61, pages 243-253

Hiramatsu Y. (2022) Seismic activities and seismotectonics in the northern Noto Peninsula, Geography and Crustal Dynamics Research Center,Geospatial Information Authority of Japan, Report of the coordinating committee for earthquake prediction, Vol. 107, 12-10 (in Japanese)

Itaya T. and Okada T. (1995) The past, present and future of the K-Ar method in Quaternary research, The Quaternary Research, Vol. 34 (3), pages. 249-259 (in Japanese)

Japan Weather Association (2011) Summary of the 2011 Tohoku-Pacific Ocean Earthquake Tsunami (3rd Report) Tsunami height and inundation height from Aomori to Fukushima Prefectures and inundation from Aomori to Chiba Prefectures (in Japanese)

Käßner A. Stanek K. and Lapp M (2020) Post-Variscan tectonic and landscape evolution of the Elbe Fault Zone and the Lusatian Block based on apatite fission-track data and geomorphologic constraints, Geomorphology, Vol. 355, https://doi.org/10.1016/j.geomorph.2019.106860

Kato A. Nakamura K. and Hiyama Y. (2016) The 2016 Kumamoto earthquake sequence, Proc. Jpn. Acad., Vol.92, No.8, pages 358-371

Lee H. and Yang J. (2003) ESR dating of the Wangsan fault, South Korea, Quaternary Science Reviews, Vol. 22, Issues 10-13, pages 1339-1343, https://doi.org/10.1016/S0277-3791(03)00018-0

Lyons, J. B. and Snellenburg, J. (1971) Dating Faults, Geological Society of America Bulletin, 82, 6, 1749-1752.

Ministry of Land, Infrastructure, Transport and Tourism (2021) Collapsed area of the Hokkaido earthquake and comparison with past earthquake disasters,

Mori S. and Kazuni S. (2005) Consideration concerning cause of Shinkansen derailment in Niigataken Tyuetu Earthquake, Proc. 28th JSCE Earthquake Engineering Symposium, page 183-188 https://doi.org/10.11532/proee2005.28.183 (in Japanese)

Murakami Y. Mizugaki S. and Fujinami T. (2020) Total number and area of collapsed areas in the Hokkaido earthquake of 2008, Japan Society of Erosion Control Engineering Hakkaido (in Japanese)

Muramatsu T. (1987) Absolute dating by the fission track method, Niigata Prefectural Education Centre Research Report, Vol. 93 pages 47-50

Odagiri S. and Shimazaki K. (2001) Correspondence of a Historical Earthquake to a Seismogenic Fault, The Earthquake, Vol. 54, pages 47-61 (in Japanese)

Pleuger J. Mancktelow N. Zwingmann H. and Manser M (2012) K–Ar dating of synkinematic clay gouges from Neoalpine faults of the Central, Western and Eastern Alps, Tectonophysics, Vol. 550-553, Pages 1-16, https://doi.org/10.1016/j.tecto.2012.05.001

Qiu D. Liu Q. Yun J. Jin Z. Zhu D. Li T. and Sun D. (2018) Electron spin resonance (ESR) dating of pre-Quaternary faults in the Sichuan basin, SW China, Journal of Asian Earth Sciences, Vol. 163, pages 142-151, https://doi.org/10.1016/j.jseaes.2018.06.011

Spencer J. Hadizadeh J. Gratier J. and Doan M (2012) Dating deep? Luminescence studies of fault gouge from the San Andreas Fault zone 2.6 km beneath Earth's surface, Quaternary Geochronology, Vol. 10, pages 280-284, https://doi.org/10.1016/j.quageo.2012.04.023

Sueoka S. Ikuho Z. Hasebe N. Murakami M. Yamada R. Tamura A. Arai S. and Tagami T (2019) Thermal fluid activities along the Mozumi-Sukenobu fault, central Japan, identified via zircon fission-track thermochronometry, Journal of Asian Earth Sciences: X, Vol. 2, https://doi.org/10.1016/j.jaesx.2019.100011

Suzuki Y. and Watanabe M. (2006) Contribution of tectonic geomorphology toward both identifying surface earthquake fault of the 2004 Mid-Niigata Prefecture earthquake and discussing disaster mitigation, E-journal GEO,Vol.1 (1), pages 30-41, https://doi.org/10.4157/ejgeo.1.30

Sun T. Wang K. Fujiwara T. Kodaira S. and He J. (2017) Large fault slip peaking at trench in 2011 Tohoku-oki earthquake, NatureCommunications, 8, Article number: 14044 DOI: 10.1038/ncomms14044

Tamura H. and Sato Y. (2013) K-Ar geochronology of faults, geological technology, geological technologyol. 3, pages 21-25 (in Japanese)

Yamada R. Matsuda T. and Omura K. (2007) Apatite and zircon fissiontrack dating from the Hirabayashi-NIED borehole, Nojima Fault, Japan: Evidence for anomalous heating in fracture zones. Tectonophysics, 443, 153-160.

Yamazaki H. (1998) Active faultsand the mitigation of earthquake hazard, The Geological Society of Japan, Vol. 51, pages 135-143, http://dl.ndl.go.jp/info:ndljp/pid/10810257

Zwingmann H. Yamada K. and Tagami T. (2010) Timing of brittle deformation within the Nojima fault zone, Japan, Chemical Geology, 275, 176-185

CHAPTER 2

2. Thernoluminescence dating of active faults: application to the Nojima Fault

2.1 Introduction

Japan is one of the most earthquake-prone countries in the world. A recent example is the 2011 earthquake off the Pacific coast of Tohoku (M = 9.0), which caused enormous damage. Many of these earthquakes are caused by active faults. For example, the Nojima Fault, an active fault on Awaji Island, Hyogo Prefecture, is recognised as the epicentre of the 1995 Hyogo-ken Nanbu earthquake (M = 7.3), and its hypocentre was estimated to be 16.0 km deep (Mizoguchi et al., 2008).

Extensive research has been conducted on the Nojima fault. This includes fault-related rock classification using drilled cores (Tanaka et al., 1999), displacement studies (e.g. Ikeda et al., 1995; Lin et al., 1995), transmission electron microscopy to observe microscopic crystalline flakes in amorphous materials (Christoph et al., 2013), and observation of frictional heat during fault activity (Gotoh et al., 1997). Various age-dating techniques have been used to study the history of fault activity, including electron spin resonance (ESR) (e.g. Fukuchi et al., 1997), K-Ar method (e.g. Zwingmann et al., 2010), fission-track method (e.g. Murakami and Tagami, 2004; Yamada et al. 2007; Ito et al., 2010), U-Pb method, U-Th method (Watanabe et al., 2008) and U-Th/He method (Ito, 2006).

Luminescence dating is based on the trapping of electrons produced by natural and cosmic ionising radiation by impurity centres in mineral crystals. The amount of electrons captured is proportional to the exposure dose and is equal to the dose accumulated since the past event that reset the signal (equivalent dose [De]) (Aitken, 1985). The trapped electrons recombine with a partner hole and emit light when stimulated by heat or light (Aitken, 1985, Tsukamoto et al., 2005, Obata et al., 2015). The thermoluminescence (TL) method measures the intensity of the emission when the sample is heated. The natural radiation absorbed by the minerals in one year (annual dose [AD]) is measured at the sample site or calculated from the concentration of radio nuclides, and the age is defined as De divided by AD.

Compared with the ESR and K-Ar methods, signal reset occurs in a very short time even at low temperatures in luminescence dating, and it has the potential to identify the time of final faulting activity (Ganzawa et al., 2013), as faulting should cause frictional heating and thus erase the accumulated luminescence signals.

In this study, we investigate the effect of faulting activity on the TL signal using quartz samples obtained from the fracture zone found during the 2017 trench survey of the Nojima Fault conducted by the Nuclear Regulation Authority, and test whether the final activity of an active fault can be detected by the luminescence method.

2.2 Nojima Fault and the analyzed samples

The Nojima and Asano active faults extend from northeast to southwest in the northern part of

Awaji Island, southwestern Japan (Figure 2-1). The Nojima fault is about 7 km long from Esaki to Hikinourain in the northeast part, and the southwest part is called the Asano fault (Mizuno et al., 1990). These faults form the southwestern part of the Rokko-Awaji Island fault system, which is 2-5 km wide and 70 km long at the boundary between the subsiding Osaka Bay and the uplifted Rokko Mountains and Awaji Island (Okada, 1995a). This fault system was active during the Quaternary (e.g. Fujita and Kasama, 1971, 1982, 1983, Fujita and Maeda, 1984) and is currently a right-lateral fault (Agatsuma, 1997). The recurrence interval of the fault is estimated to be about 2,000 years (Kurita and Mizuno, 1998).

The northern part of Awaji Island consists of granitic rocks, the Kobe Group and the Pliocene and Pleistocene Osaka Group. The Nojima and Asano faults form the boundary between the Cretaceous granitoids and the Kobe and Osaka Groups (Yamada et al., 2007). Terrace deposits on sedimentary rocks are also cut by the Nojima fault (Ishizawa et al., 1997).

The 1995 Hyogo-ken Nanbu earthquake (M = 7.3) occurred at 5:46 a.m. on 17 January 1995, with an epicentre near the northeastern part of Awaji Island (the depth of the hypocentre was about 16 km). Significant surface displacement was detected along the Nojima fault (Nakata et al., 1995). The maximum vertical displacement caused by the earthquake was 1.0-1.2 m, and the horizontal displacement was 1.9-2.1 m (right lateral) (Nakata et al., 1995, Ikeda et al., 1996a). The near-surface dip of the fault plane was about 70°SE-80°SE in the Ogura area, where the study was conducted.

The trench survey was conducted at a site 720 m east-southeast of the Hokudan Earthquake Memorial Park in Ogura, Awaji City, with dimensions of 15 m long in a northwest-southeast direction, 2.5-5 m wide (Figure 2-2), and 1.5-3 m deep.

Faulting was observed on the northern and southern walls of the trench. The fault gouge was found between the granitic breccia and the sedimentary rocks. The main fault gouge was about 2-4 cm thick, with a strike of N36°E-N38°E and a dip of 62°W-65°W. Several well defined fractures were found in the granitic breccias. The granite breccias have been altered and are easily broken with a hammer. The sedimentary sequence is composed of clay and silt and contains pebbles about 2-100 mm in diameter. This sedimentary sequence belongs to the Osaka and Kobe Groups.

Samples were collected from the south wall of the trench (Figure 2-2). One sample was collected from the gouge and seven samples were collected from the granitic breccia zone at 1m intervals to the east of the gouge (S1-S7 from east to west). S7 was collected from within a few millimetres of the gouge sample. In addition, a sample was collected from the eastern wall of the trench (E1), the furthest from the fault in the trench. All of these samples were affected to some extent by fault activity. We also collected two basement granite samples that were less affected by fault activity. One was from about 200 m east of the trench (base rock [BR]) and the other from about 3 km from the fault in the Tsushigawa granite (TS). All these samples were collected after removing 30 cm of rock (in thickness) from the surface under a dark sheet to avoid exposure to light.

All samples were processed in a dark room to prevent reduction of the luminescence signal due to exposure to light. After crushing, the samples were first treated with hydrochloric acid (1 M, 10 min), followed by hydrofluoric acid (25%, 10 min). Finally, they were washed with ion-exchanged water and dried. All quartzes smaller than 250 μm were used for the measurement. X-ray diffraction (XRD; Ultima IV: CuKα, 40 kV, 30 mA; Rigaku Corp., Tokyo, Japan) was used to determine the mineralogical compositions of the selected samples (TS, E1, S7) (Kitajima et al., 2020).

2.3 Luminescence measurement

2.3.1 Devices

The luminescence measurement system used in this study is a modified version of the one used in Ganzawa et al. (2013) and was equipped with photomultiplier tubes (Hamamatsu Photonics: R585s) with excellent reception in the ultraviolet (UV) to blue luminescence emission. The filter used was RR0340 (Asahi Spectroscopy). This filter has a lower transmittance in the infrared region than U340, which is used in conventional optically stimulated luminescence (OSL) measurements. Therefore, TL was detected in the UV region (UV-TL). An x-ray source (Varian: VF-50) was used to provide an artificial dose (Hashimoto et al., 2002).

2.3.2 TL measurement

Several tens of quartz particles per aliquot were used for TL measurements. The equivalent doses were determined using the single-aliquot regenerative dose (SAR) method (Wintle and Murray, 2006).The temperature range for the SAR TL measurements was 100°C-450°C, and the preheat temperature (PH) was set at 220°C for 10 s (Table 2-1). This PH condition was chosen to compare the results with the OSL measurements to be made by others on the same sample in the future.

2.3.3 Characteristics of the luminescence sites

Prior to TL dating, the T-Tmax method (McKeever, 1980) was applied to selected samples (BR, TS, E1 and S7) to determine the quartz luminescence sites and their signal emitting temperatures. The T-Tmax method is a technique for estimating the peak temperature of a luminescence signal by gradually changing the preheat temperature. The TL emission curve was decomposed using a Gaussian function to obtain the emission curve of each luminescence site. The preheat temperature was set at 10°C intervals from 100°C to 450°C and repeated measurements were made on the same aliquot. The measurement procedure for the T-Tmax method is shown in Table 2-2.

The lifetime () of each emission site was calculated from E1 and BR. The trap depth (E:eV) and the frequency factor (s:1/s) for the calculation of τ were determined using the peak shift method (Aitken, 1985, equation 1). This method observes the increase in temperature of the luminescence emission by increasing the heating rate in the TL measurement. The heating rate was set between 1

and 4 K/s.

$$\ln(T\text{m}^2/\beta) \;=\; E/kT\text{m} - \ln(sk/E) \quad (1)$$

where Tm is the luminescence site temperature (K), β is the heating rate (K/s), E represents the trap depth (eV), k is the Boltzmann's constant (8.615×10^{-5} eV/K), and $s$is the frequency factor (1/s). Then, we used the following equation to calculate the lifetime τ.

$$\tau \;=\; s^{-1}\exp(E/kT) (2)$$

2.3.4 Fading test

The fading of the TL signals was investigated. The experimental procedure was as follows: After a natural TL measurement, a sample was irradiated with X-rays (100 Gy) and left in a dark room at room temperature for a specified time (up to 2000 h). The TL signal was then measured and the procedure repeated. The signal obtained from the first measurement was used as the standard.

2.4 Annual dose measurement

K_2O concentrations were measured using X-ray fluorescence analysis (ZSX primus II, Rigaku Corporation) (Kusano et al., 2014) and calculated by converting the concentration to 100% to account for ignition loss. The radioelement concentrations (U, Th and Rb) were measured by laser ablation inductively coupled plasma mass spectrometry (LA-ICP-MS: Yokogawa Analytical Systems Agilent 7500s equipped with MicroLas GeoLas Q-Plus), and the annual doses were calculated using the obtained values (Ito et al., 2009; Tamura et al., 2015). The experimental details are described in Ito et al. (2009). The effect of -rays was not considered in the calculation of the annual dose because the samples for the luminescence measurement were treated with hydrofluoric acid to remove the outer shell of the quartz particles. The annual dose for the outcrop samples also took into account the cosmic dose (Prescott and Hutton, 1994).

2.5 Result and discussions

2.5.1 Analyzed mineral assemblage

The XRD results are shown in Figure 2-3. The results of the measurements indicate that the samples are composed almost entirely of quartz.

2.5.2 Luminescence site and lifetime

Four luminescence sites were identified by the T-Tmax method (Figures 2-4 (a) and (b)). The TL emission temperatures were approximately 200°C, 270°C, 340°C and 400°C at a heating rate of 1 K/s.

We refer to these luminescence sites as sites 1 to 4 from low to high temperatures. The signal from site 4 was not pronounced. This may be due to the low irradiation dose (100 Gy) used to determine the luminescence sites. Although a higher dose may be useful in identifying site 4, the high dose may affect the shape of the glow curve and was avoided.

The glow curves of sample S7 were different from those of the other three samples (Figs. 2-4 (c) and (d)). No clear luminescence sites were identified in this sample. However, in this study we calculated the accumulated dose for all samples by decomposing the peaks using the temperature of the luminescence sites obtained from the other samples.

The luminescence curves for the peak shift method obtained at different heating rates are shown in Fig. 2-5. By increasing the heating rate during the TL measurement, the luminescence emitting temperatures are shifted to higher temperatures. Using this measurement result and equation (1), the trap depth (E: eV) and the frequency coefficient (s:1/s) were calculated (Table 2-3). The data from Spooner et al. (2000) were used as reference data. The E value of site 2 was very close to the E value of 325°C calculated by Spooner et al. (2000).

The temperature obtained by Spooner et al. (2000) is higher because they used a heating rate of 5 K/s. This site is considered to be an important luminescence site linking TL and OSL and should be focused on in the future.

The resultant value calculated using the data from E1 is plotted against the ambient temperatures for each luminescence site in Figure 2-6. The result shows that the luminescence signal is sensitive to brief heating in the order of seconds. The value was low for luminescence sites emitting at low temperatures. Therefore, low temperature luminescence sites are useful for dating active faults. However, if the value is too low, the site could be unstable on a geological time scale and this should be taken into account when interpreting the TL signal profile.

2.5.3 Fading

During the fading test, the samples were repeatedly irradiated and heated. However, there was no change in peak temperatures even after 2000 hours of storage (Figure 2-7). Fading was observed in the site 1 signal. Therefore, the luminescence from site 2 was the most preferable for calculating the accumulated dose to determine the reset age by frictional heating.

2.5.4 Shape of the luminescence signal

Figure 2-8 shows an example of the TL signal measurements for Gouge and BR. The natural glow curves of both samples are similar, with a peak at around 300°C. The other samples (TS, E1 and S1 to S6) also showed similar natural glow curves, but almost no natural glow was detected in S7. A common feature in the shape of the natural glow curves is that the signals do not accumulate at lower temperatures (around 240°C), suggesting that the signals from Site 1 may be unstable over long time

scales. In the natural glow curves of S1-S6, the contribution of luminescence at site 4 (400°C) was stronger than the regenerative signal.

The shape of the luminescence glow curve after regenerative irradiation can be classified into two types: one with strong emission at 340°C, as seen for sample BR (Fig. 2-8 (a)), and the other with maximum emission around 240°C, as seen for the Gouge sample (Fig. 2-8 (b)). The emission at this temperature is a combination of the emissions from sites 1 and 2. E1 and S5 show similar regenerative glow curves to those of BR and the others to those of the gouge. The regenerative glow curve for S7 was very different from the others. It showed an emission only at about 200°C, and the intensity was more than 10 times higher than that of the other samples (Fig. 2-4 (c)).

2.5.5 Accumulated dose

The results of the accumulated dose measurements for all samples are shown in Table 2-4.

The accumulated dose from Site 1 was the lowest for all samples. The accumulated dose from Site 4 was the highest for all samples except the gouge sample. Samples TS and BR, which are considered to represent the original accumulated dose of the granite as they have not been affected by faulting, show similar De values for sites 2 and 3. Data from site 1 were very limited as the site was unstable according to the results of the lifetime calculation mentioned above. Data from site 4 differed between the two samples, but were unreliable due to their small signals. Therefore, the accumulated doses of the TS and BR samples were taken as the maximum values for the granite.

The results of E1 and S1 to S6 are discussed next. Although these samples were taken from the same granite, the resulting doses were significantly different. In particular, the variation in the accumulated doses at Sites 2 and 3 is noteworthy, suggesting that some fault activity factor may have influenced the accumulated doses. Meanwhile, the data from site 4, which was estimated on the basis of emissions at high temperatures (around 400°C), remained the largest dose, although some differences in the accumulated dose were observed.

The accumulated doses of the chisel samples are discussed next. The accumulated doses at all sites were the lowest compared to the results for the other samples, except for site1. This suggests that the accumulated doses may have been reset by fault activity. In particular, the low accumulated dose value at Site4 was evident, suggesting that there was fault activity in the past at a certain temperature that reset the signal at Site4.

Finally, a discussion of S7 is presented. This sample is the only one with a low natural emission. Only small amounts of luminescence were detected at the temperatures of sites 3 and 4. This low natural luminescence emission may be due to the resetting of the natural accumulated doses by fault activity. The signal at site 4 requires a temperature of about 450°C (for 3 s) to reduce the accumulated dose to 1/e of the original dose. It is likely that the sample has experienced such a high temperature during previous fault activities.

The different shapes in the regenerated glow curve and the strong luminescence emission found in the regenerated glow curves may be due to the change in the luminescence site caused by the fault activities. The signal at site 4 requires a temperature of about 450°C (for 3 s) to reduce the accumulated dose to 1/e of the original dose. It is likely that the sample was exposed to such a high temperature during previous perturbations. The different shapes in the regenerated glow curve and the strong luminescence emission found in the regenerated glow curves may be due to the change in the luminescence site caused by the fault activities.

Although the S7 and gouge samples were adjacent at the time of collection, these two samples may have been separated before the last fault activity. Therefore, even if the temperature around S7 reached a temperature that reset the natural signal, the temperature around the gouge may not have reached as high as that of S7. The gouge has been damaged many times in the past by frictional movement caused by fault activity, and is now easily deformed when subjected to stress. Therefore, the gouge did not experience large frictional forces and did not generate frictional heat to completely reset the signal. In contrast, S7 is hard enough and may have generated high temperature frictional heat.

2.5.6 Annual dose

The annual dose results are presented in Table 2-5. Annual doses were measured for TS, E1, S5 and S7. The K_2O concentration of all four samples was in the range of 4% to 5%. However, for the other elements, particularly U and Th, there was a large variation between samples, even for E1, S5 and S7, which were collected at relatively short distances. This suggests that these minor elements are contained in specific mineral phases in the granite and whether these minerals are present in the treated sample controls the results. It would therefore be preferable to measure the annual dose at the site close to the measured sample using a large number of samples. In this study, weighted averages of element concentrations were calculated and used to estimate annual doses for the trench samples (AD = 9.4 ± 0.7 Gy/kyr). For the outcrop samples, the annual dose was calculated by adding the dose from cosmic rays.

2.5.7 Age estimate

The ages calculated for the four luminescent sites are shown in Table 2-6. The age of the signal from site 1 was by far the youngest compared to the other sites. The value for Site 1 indicates that the signal is very short-lived and unstable even at room temperature (about 120 years at 25°C). Therefore, the age inferred from Site 1 may not be a geologically meaningful age.

The age of the granite in this area is referred to as the basement rock age (TS and BR) (Table 2-5, Figure 2-9). The ages from sites 2, 3 and 4 were 35-40, around 40 and 80-145 ka respectively. These ages are too young for the age of the granite formation and may indicate past uplift of the granite to

the surface. The age difference between the BR and TS of the Site 4 emission may indicate different past uplift processes.

For the trench samples (E1 and S1 to S6), the ages calculated from the TL signal of the Site 2 emission were generally around 45 ka, although there were some variations. The age values for Site 3 varied widely. Neither Site 2 nor Site 3 ages were close to those of the gouge sample.

The gouge sample was older than the expected date of last activity of 30 years. This suggests that the samples have not experienced sufficient heat to completely reset the TL signal at the time of last activity. If the samples were collected from a depth with a high ambient temperature, the emission signal could have been reset by heat generated by friction (Oohashi et al., 2020). Sample S7 had an age closer to the last fault activity than the other samples in this study. The S7 sample may have received enough heat to reset the signal.

2.6 Summary

In this study, we performed TL measurements on quartz samples collected from the fracture zone of the Nojima fault. We evaluated the TL sites of the samples and investigated whether it is possible to identify the last active period of the active fault by calculating the accumulated dose at each luminescence site. Identifying the last active period of an active fault requires the use of luminescence sites that are stable on the geological time scale but reset at lower temperatures.

Consequently, the ages calculated from the gouge samples did not agree with the expected age of the last fault activity of about 30 years. However, the age of S7 is more or less consistent with the last activity. Further investigation is needed into why the signal was lost from S7 but not from the gouge samples, and how the samples were thermally damaged during the faulting. In any case, more detailed studies of how deformation during faulting affects luminescence sites and accumulated signals are needed.

So far, we have considered the shape of the glow curves and accumulated dose estimates to assess the effect of fault activity. The difficulties in estimating annual dose, especially for the granite samples analysed here, also pose a challenge for luminescence dating of fault activity.

The different ages of the trench samples from those of the basement samples suggest that signals have been lost or even created in the past. Although we were not able to identify the cause of the age difference in this study, we can explore this further in future studies.

Many previous fault studies have discussed the energy released by faults (e.g. Kaneko et al., 1997, Shimamoto et al., 2003, Mori et al., 2009). However, these studies calculated the total energy in the active fault zone and the frictional heat at depth, but not the energy at a specific location near the ground surface, such as the locations of the samples used in this study. Luminescence measurements can estimate the amount of heat generated locally and can help to understand the physical processes occurring in fault zones.

2.7 Acknowledgments
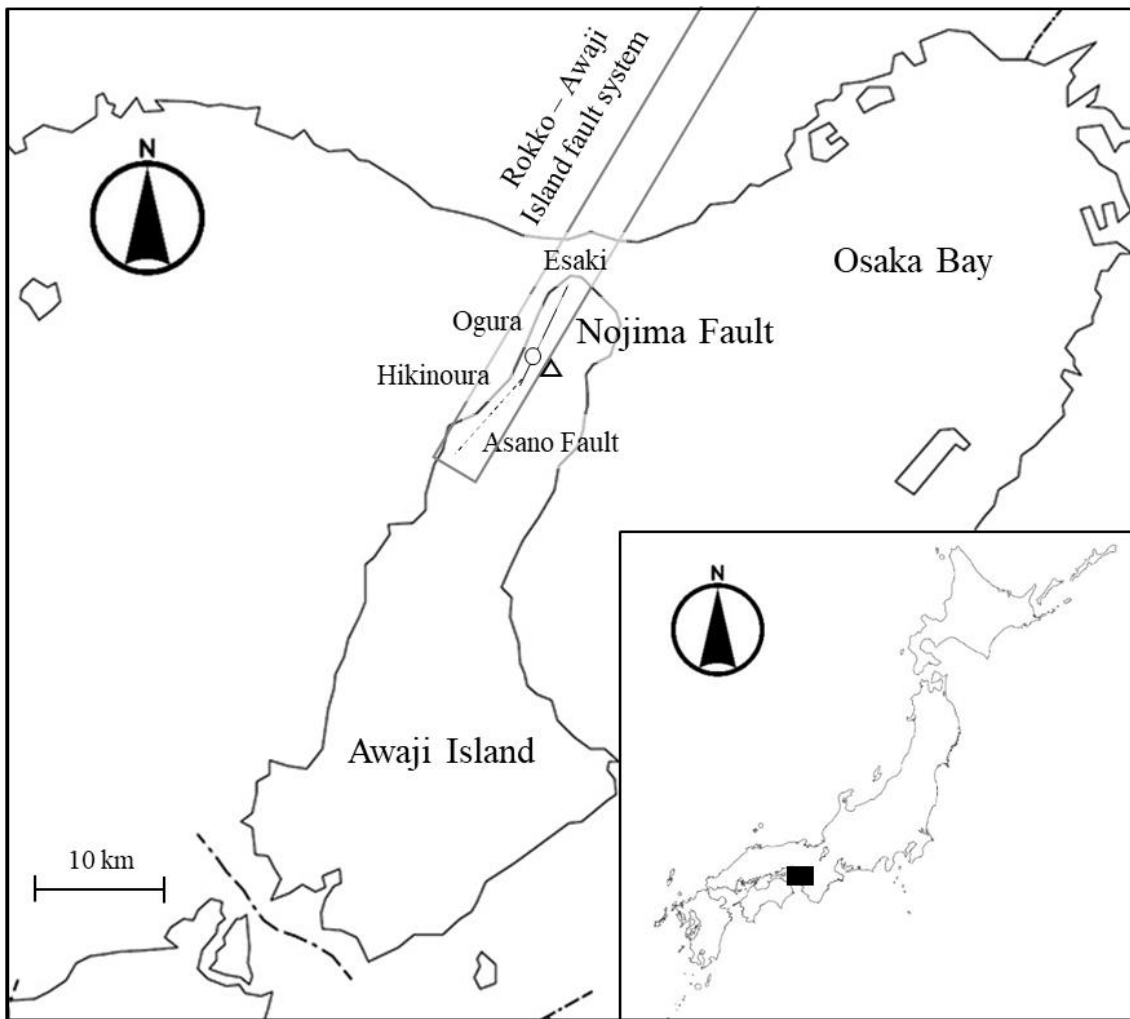
Figure2-1. Sample localities. The Nojima Fault is an active fault extending approximately 7 km from Esaki to Hikinoura. The southern part of the Nojima Fault (solid line) is connected to the Asano Fault (dotted line). These faults belong to the southern part of the Rokko–Awaji Island fault system (square frame). The open circle is the location of the trench, and the open triangle is the location from where the Tsushigawa granite (TS) was collected. The base rock (BR) was sampled about 200 m east of the trench.
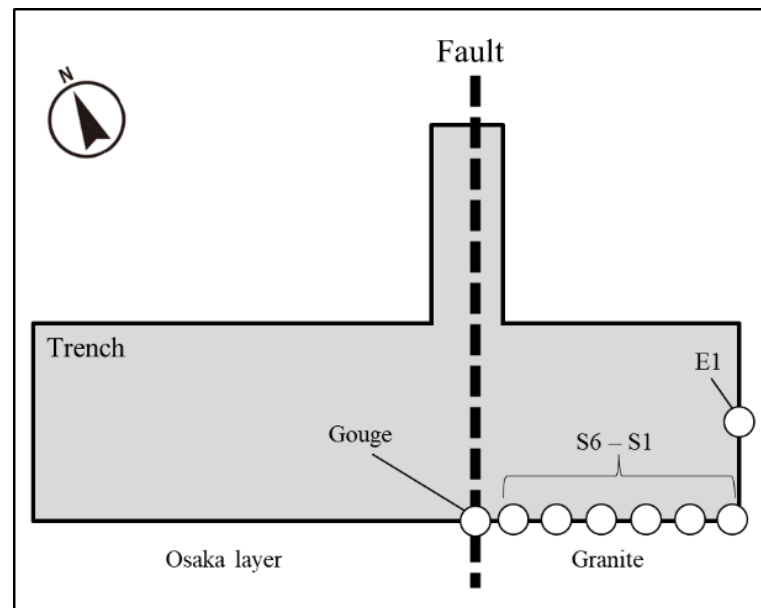
Figure2-2. Schematic image of the trench where the samples were collected.
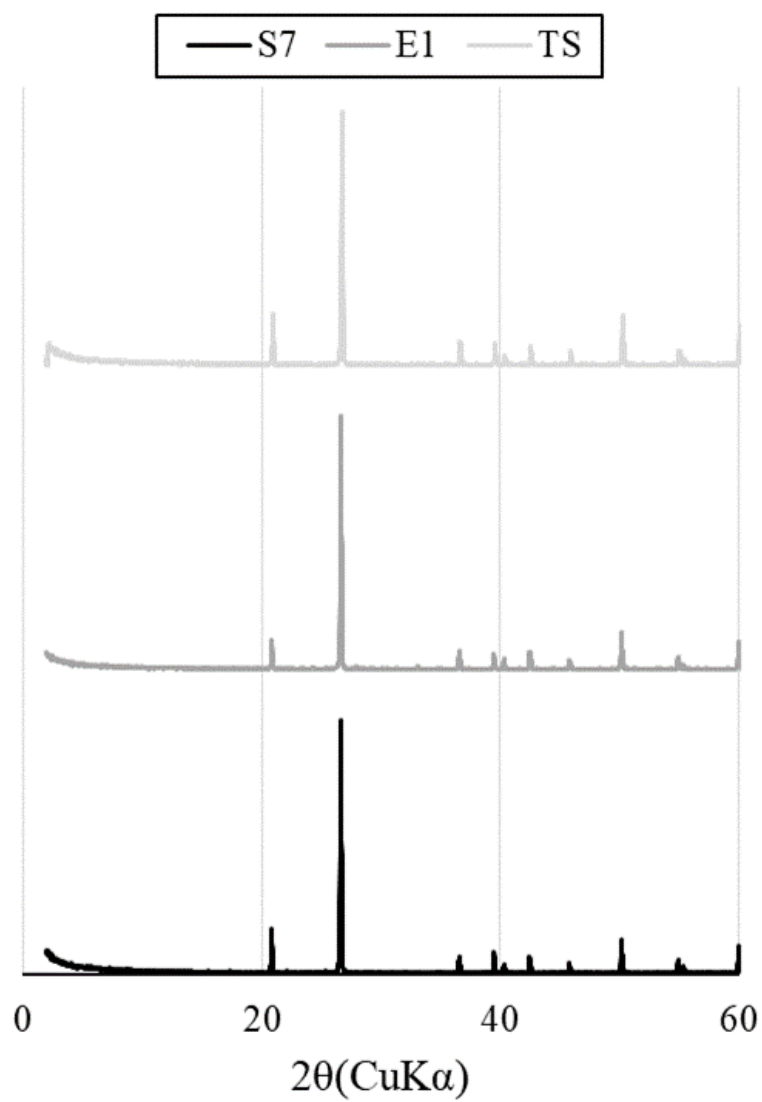
Figure2-3. Results of the XRD analyses.
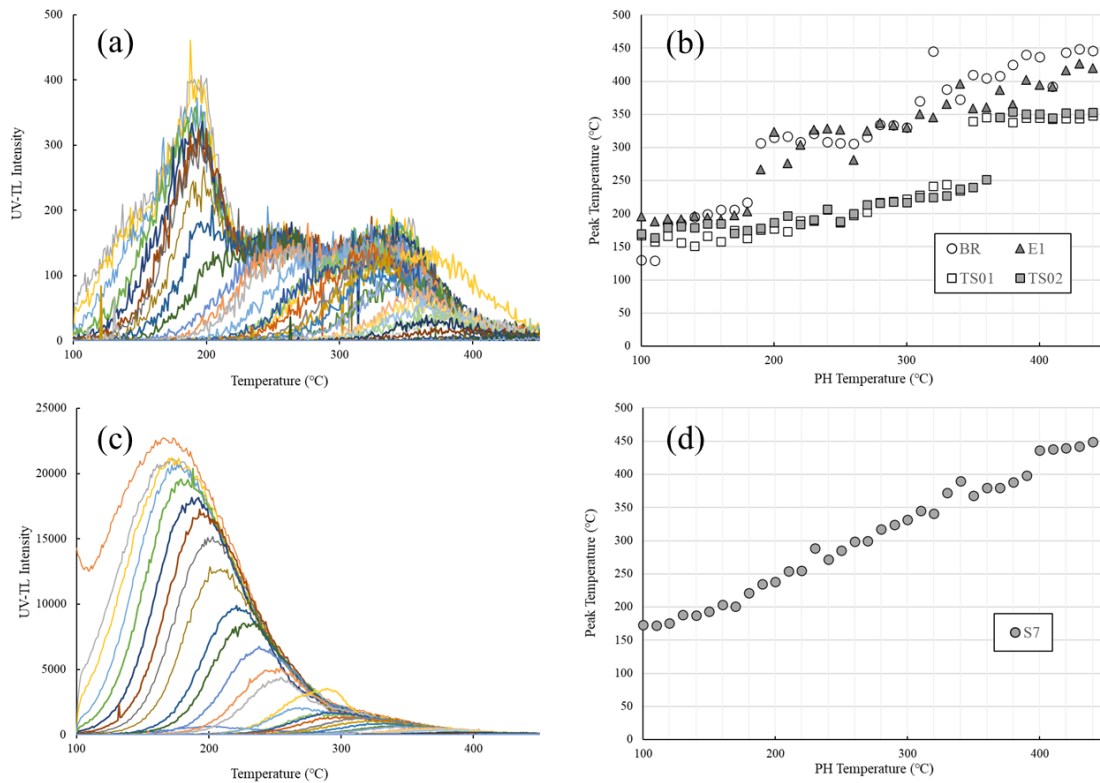
Figure2-4. Results of the T–Tmax measurements. (a) Example of glow curves (E1). The preheat temperature was increased every 10° from 100°, and the TL was measured. (b) The lowest peak temperature in the glow curves is plotted against the PH temperatures for three samples (BR E1, and TS). Two aliquots were measured for TS. (c) T–Tmax emission curves from S7. (d) The lowest peak temperature of the S7 glow curves plotted against PH temperatures. The results show no clear luminescence sites
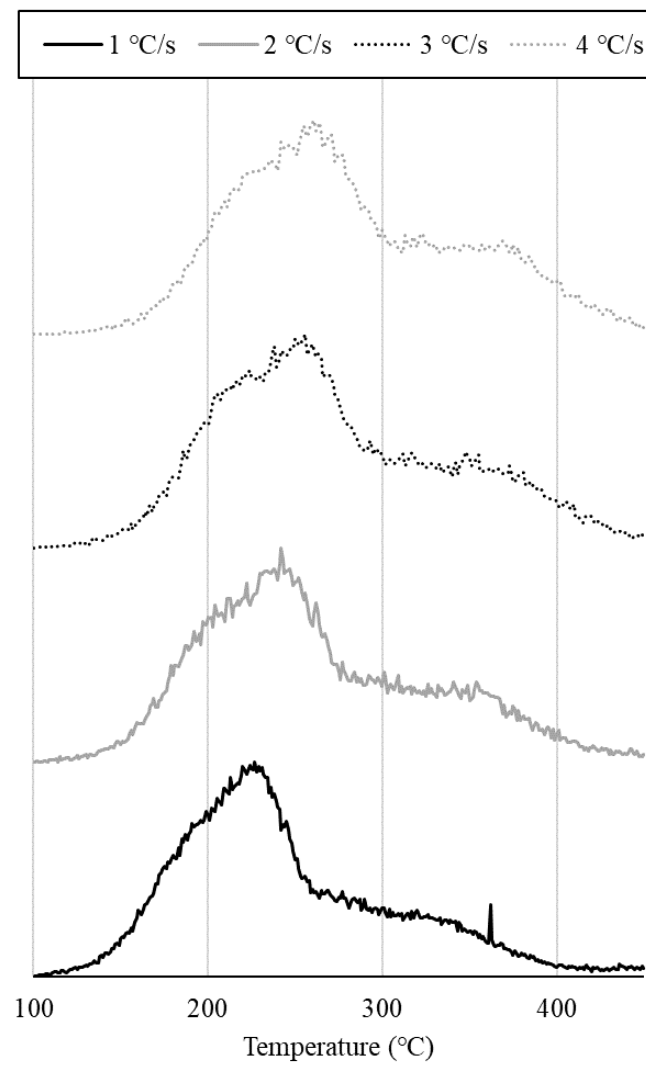
Figure 2-5. Luminescence emission curves measured using
the peak shift method. As the heating rate increases, the peak
luminescence temperatures shift to higher temperatures.
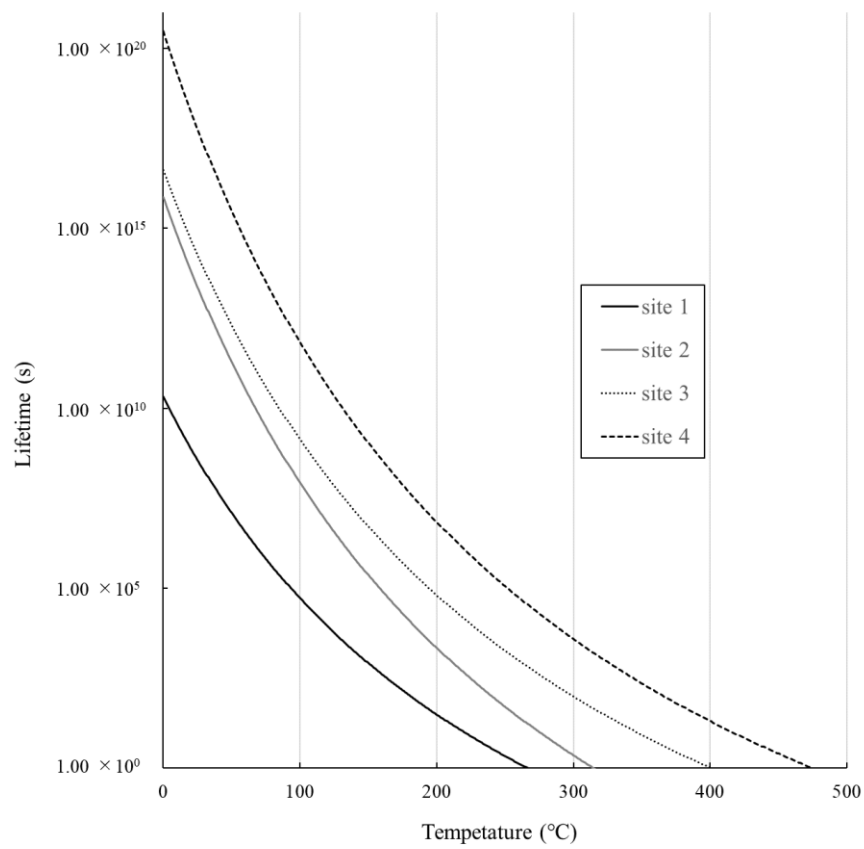
Figure2-6. Lifetime (τ: s) of the luminescence site calculated for sample E1 under particular ambient temperatures.
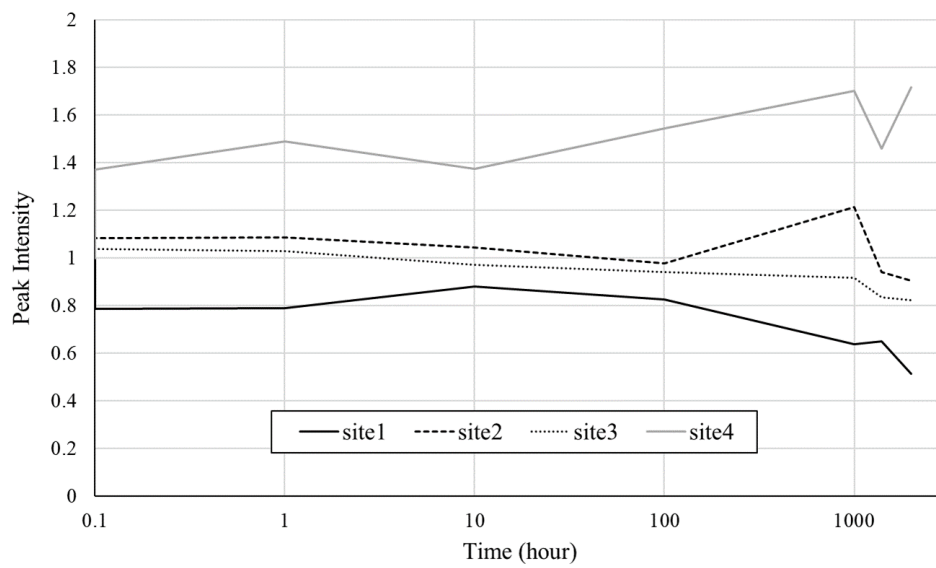
Figure2-7. Results of the fading test. Normalized signal intensity is plotted against the storage

time (measured after 0.1, 1, 10, 100, 1000, 1400, and 2000 h of storage).
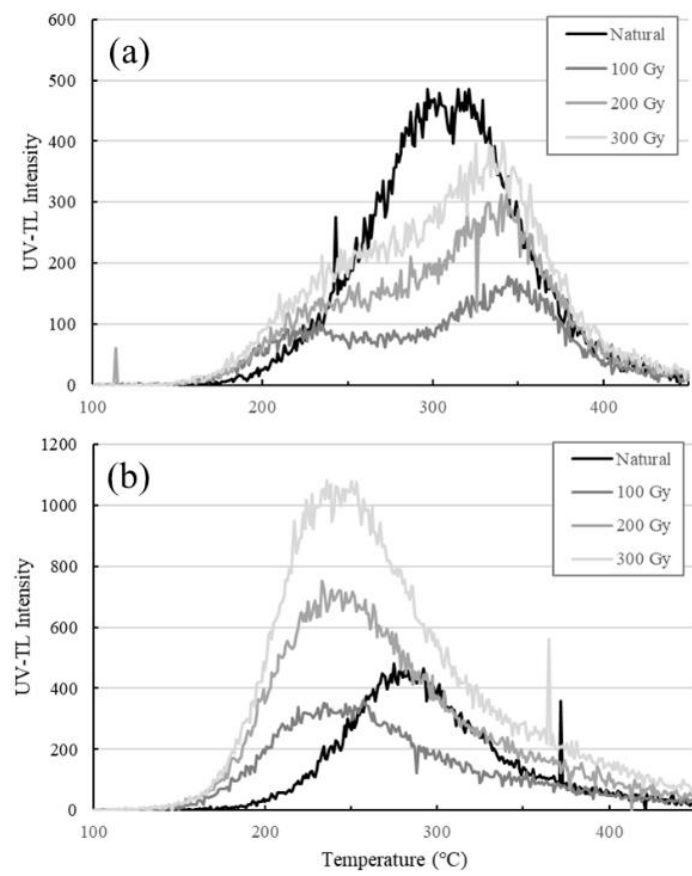
Figure2-8. Luminescence glow curves. (a) Data from BR. (b) Data fault gouge.
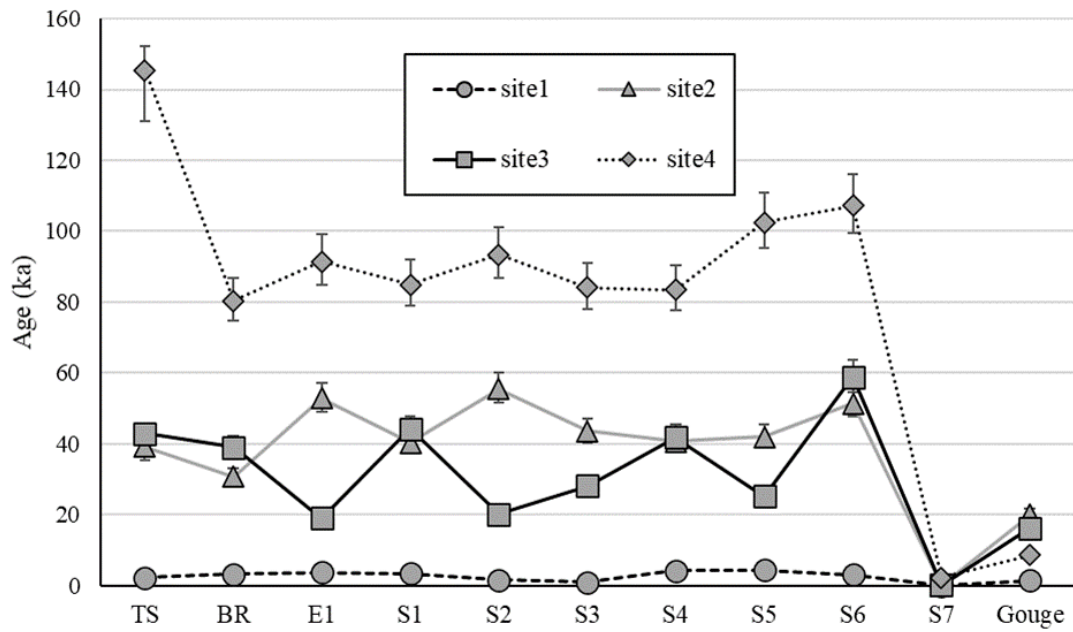
Figure2-9. Age estimate results.

Table 2-1 TL measurement protocol used to estimate the equivalent dose (De)

	Treatment
1	PH (220°C × 10s)
2	TL measurement (100 - 450°C)
3	Irradiation test dose
4	PH (220°C × 10s)
5	TL measurement (100 - 450°C)
6	Irradiation dose
7	Return to 1

Table 2-2 T–Tmax measurement protocol

	Treatment
1	Irradiation dose (100Gy)
2	PH (no PH, 100-440°C × 10s)
3	TL measurement (100-450°C)
4	Irradiation dose (50Gy)
5	PH (220°C × 10s)
6	UV-TL measurement (100-450°C)
7	Returun to 1

Table 2-3 The trap depth and frequency factor calculated using the peak shift method

Luminescence site		E (eV)	s (1/sec)
BR	site1 (200°C)	1.18 ± 0.01	$1.24 \times 10^{11} \pm (\times 10^{0})$
	site2 (270°C)	1.62 ± 0.23	$8.23 \times 10^{13} \pm (\times 10^{2})$
	site3 (320°C)	1.57 ± 0.13	$6.60 \times 10^{11} \pm (\times 10^{1})$
	site4 (400°C)	1.75 ± 0.25	$5.99 \times 10^{11} \pm (\times 10^{2})$
E1	site1 (200°C)	1.13 ± 0.17	$3.73 \times 10^{10} \pm (\times 10^{2})$
	site2 (270°C)	1.61 ± 0.14	$5.77 \times 10^{13} \pm (\times 10^{2})$
	site3 (320°C)	1.51 ± 0.11	$7.20 \times 10^{10} \pm (\times 10^{1})$
	site4 (400°C)	1.75 ± 0.25	$5.99 \times 10^{11} \pm (\times 10^{2})$
Spooner et al., (2000)	220 °C (5K/s)	1.63	3.40×10^{16}
	280°C (5K/s)	1.50	1.50×10^{13}
	325°C (5K/s)	1.65	3.90×10^{13}

Table 2-4 Results of the accumulated dose measurements for each luminescence site

De (Gy)	TS	BR	E1	S1	S2	
site1	21.0	32.4	35.3	32.4	14.8	
site2	370.3	298.9	499.0	380.6	523.8	
site3	404.6	379.2	179.7	416.9	189.8	
site4	1371.0	781.4	861.7	800.4	879.8	
	S3	S4	S5	S6	S7	Gouge
	9.3	40.0	42.2	28.6	0.1	14.0
	410.3	383.7	395.0	485.2	0.5	189.0
	266.0	394.4	238.2	554.7	1.5	153.0
	792.3	787.5	965.5	1011.1	21.3	81.9

Table 2-5 Results of the radioelement measurements and estimates of the annual doses

	K_2O (%)	Rb (ppm)	SE (ppm)	Th (ppm)	SE (ppm)	U (ppm)	SE (ppm)	AD (Gy/kyr)	Error (%)	cosmic ray (Gy/kyr)
TS	4.2	391.5	9.2	45.1	20.6	8.9	0.2	9.9	45.8	
E1	4.3	297.4	22.1	11.9	1.6	2.9	0.6	5.8	24.5	
S5	5.0	226.9	22.8	88.7	11.3	15.4	3.9	15.0	30.2	0.3
S7	4.4	189.2	15.8	27.6	3.2	3.3	0.6	6.7	22.3	
Weighted mean and error	4.5	363.4	7.7	42.8	3.0	8.8	0.2	9.4	7.7	

Table 2-6 Age estimate results

	TS			BR			E1			S1			S2		
site1	2.2	±	0.2	3.3	±	0.2	3.7	±	0.3	3.4	±	0.3	1.6	±	0.1
site2	39.3	±	2.9	30.7	±	2.3	52.9	±	4.1	40.4	±	3.1	55.6	±	4.3
site3	42.9	±	3.1	39.0	±	2.9	19.1	±	1.5	44.2	±	3.4	20.1	±	1.6
site4	145.4	±	10.6	80.3	±	6.0	91.4	±	7.1	84.9	±	6.6	93.3	±	7.2

S3			S4			S5			S6			S7			Gouge		
1.0	±	0.1	4.2	±	0.3	4.5	±	0.3	3.0	±	0.2	0.0	±	0	1.5	±	0.1
43.5	±	3.4	40.7	±	3.1	41.9	±	3.2	51.5	±	4.0	0.1	±	0.0	20.1	±	1.6
28.2	±	2.2	41.8	±	3.2	25.3	±	2.0	58.8	±	4.6	0.2	±	0.0	16.2	±	1.3
84.0	±	6.5	83.5	±	6.5	102.4	±	7.9	107.3	±	8.3	2.3	±	0.2	8.7	±	0.7

2.8 References

Aitken M.J. (1985) Thermoluminescence dating, Academic Press Inc. Ltd.,269-273

Fukuchi T. (1992) ESR studies for absolute dating of fault movements, Journal of the Geological Society, 149, 265-272

Fukuchi T. and Imai N. (1998) Resetting experiment of E' centres by natural faulting–The case of the Nojima earthquake fault in Japan, Quaternary Science Reviews, 17, 1063-1068

Ganzawa Y. Takahashi C. Miura K. and Shimizu S. (2013) Dating of active fault gouge using optical stimulated luminescence and thermoluminescence, The Journal of the Geological Society of Japan, 119, 714-726

Gotoh K. Jun B. and Nishikawa U. (1997) Theoretical and experimental study on ground surface temperature rise due to active fault slip, Nagasaki University's Academic Output, 27, 77-80

Grün R. Tani A. Gurbanov A. Koshchug D. Williams I. and Braun J. (1999) A new method for the estimation of cooling and denudation rates using paramagnetic centers in quartz: A case study on the Eldzhurtinskiy Granite, Caucasus, Journal of Geophysical Research: Solid Earth, 104, 17531-17549

Hashimoto T. Nakagawa T. Usuda H. and Yawata T. (2002) Development of an automated system equipped with a small X-ray irradiator for red /blue thermoluminescence and optically stimulated luminescence measurement from natural minerals, Bunseki Kagaku, 51, 625-632

Ikeda Y. Togo M. and Sawa S. (1996) Maximum slip vector on the Nojima Fault associated with the Hyogoken Nanbu, Western Japan, Earthquake of January 17 1995, Journal of the Seismological Society of Japan. 2nd ser. Zisin, 48, 531-537

Ikeya M. and Toyoda S. (1991) Thermal effect in metamorphic rock around an intrusion zone with ESR studies, Applied Magnetic Resonance, 2, 69-81

Ishizawa K. and Okabe Y. (1997) Topography, geology and active fault of the Hanshin-Awaji area, as tectonic implications to the 1995 Hyogo-ken Nanbu Earthquake, OYO TECHNICAL REPORT 1997, 19-46

Ito H. (2006) Evaluation of thermal and tectonic history of shallow crust by dating methods with low closure temperature Examples of Nojima and Yanagase faults, Central Research Institute of Electric Power Industry Report, N05060, 18

Ito H. Tamura A. Morishita T. and Arai S. (2010) Zircon U-Pb and fission-track ages of granitic rocks from the Nojima Fault and its vicinity: A new horizon for the LA-ICP-MS U-Pb dating method, The Journal of the Geological Society of Japan, 116, 544-551

Ito K. Hasebe N. Sumita R. Arai S. Yamamoto M. Kashiwaya K. and Ganzawa Y. (2009) LA-ICP-MS analysis of pressed powder pellets to luminescence geochronology, Chemical Geology, 262, 131-137

Janssen C. Wirth R. Lin A. and Dresen G. (2013) TEM microstructural analysis in a fault gouge sample

of the Nojima Fault zone, Japan, Tectonophysics, 583, 101-104

Kaneko F. Segawa S. and Toshioka T. (1997) An image of Hyogo-ken Nanbu earthquake, OYO TECHNICAL REPORT 1997, 1-17

Kitajima T. Fukushi K. Yoda M. Takeichi Y. and Takahashi Y. (2020) Simple, reproducible synthesis of pure monohydrocalcite with low Mg content, Minerals, 10,346

Kusano Y. Umino S. Kobayashi J. Mizumami T. Okuno M. and Arai S. (2014) Quantitative analysis of major elements in igneous rocks with X-ray fluorescence spectrometer "ZSX primus II" using a 1:10 dilution glass bead, Science Reports of Kanazawa University, 31-44

Lin A. Imiya H. Uda S. Iinuma K. Misawa T. Yoshida T. Abematsu Y. Wada T. and Kawai K. (1995) Investigation of the Nojima Earthquake Fault occurred on Awaji Island in the Southern Hyogo Prefecture Earthquake, Journal of Geography, 104, 113-126

McKeever S.W.S. Chen R. Groom P.J. and Durrani S.A. (1980) Dose-rate dependence of thermoluminescence response, Nuclear Instruments and Methods, 175, 43-44

Melnikov P.V. Moiseev B.M. and Shekhvatov D.B. (1989) Natural radiation parameters of Al-center in quartz (in Russian),Geokhimiya, 7, 1015-1020

Mizoguchi K. Hirose T. Shimamoto T. and Fukuyama E. (2008) Internal structure and permeability of the Nojima fault, southwest Japan, Journal of Structural Geology, 30, 513-524

Mori J. and Kano Y. (2009) The1999 Chi-Chi, Taiwan Earthquake (Mw = 7.6) and Fault zone temperature measurements to determine Fault friction, Japan Society for Natural Disaster Science, 28-2, 151-159

Morishita, T., Ishida, Y., Arai, S. and Shirasaka, M. (2005) Determination of multiple trace element compositions in thin (<30 μm) layers of NIST SRM 614 and 616 using laser ablation-inductively coupled plasma-mass spectrometry. Geostand. Geoanal. Res. 29, 107–122.

Murakami M. and Tagami T. (2004) Dating pseudotachylyte of the Nojima fault using the zircon fission-track method,Geophysical Research Letters, 31, L12604

Nakajima W. Masaoka K. Kosasa S. Morihana T. Tainosho Y. and Keizo Amano K. (1986) Ryoke granitic rocks in the northern part of the Awaji Island, The Association for the Geological Collaboration in Japan, 40, 227-237

Oohashi K. Minomo Y. Akasegawa K. Hasebe N. and Miura K. (2020) OSL signal resetting 1 of quartz gouge during sub-seismic to seismic frictional sliding; a case study using granite-derived quartz, Journal of Geophysical Research: Solid Earth, 125, e2020JB019900

Obata, N and Shitaoka Y, (2015) Introduction to the detection of heated histories using luminescence phenomena, Engineering Geology of Japan, "The special issue of 20th anniversary of Hiruzen Institute for Geology and Chronology,"5, 29-35

Prescott J.R. and Hutton J.T. (1994) Cosmic ray contributions to dose rates for luminescence and ESR dating: Largedepths and long-term time variations, Radiation Measurement, 23, 497-500.

Shimamoto T. Hirose T. Mizoguchi K. and Noda H. (2003) High-velocity friction of faults and earthquake generating processes: Current status and future perspectives, Journal of Geography, 112, 979-999

Spooner N.A. and Questiaux D.G (2000) Kinetics of red, blue and UV thermoluminescence and opticallystimulated lumines-cence from quartz, Radiation Measurements, 32, 659-666

Stokes S. Ingram S. Aitken M.J. Sirocko F. Anderson R. and Leuschner D. (2003) Alternative chronologies for Late Quaternary (Last Interglacial-Holocence) deep sea sediments via optical dating of silt-sized quartz. Quaternary Science Reviews, 22, 925-941.

Tamura A. Akizawa N. Otsuka R. Kanayama K. Python M. Motishita T. and Arai S. (2015) Measurement of whole-rock trace-element composition by flux-free fused glass and LA-ICP-MS: Evaluation of simple and rapid routine work, Geochemical Journal, 49,243-258

Tanaka H. Higuchi T. Tomida N. Fujimoto K. Ohtani T. and Ito H. (1999) Distribution, deformation and alteration of fault rocks along the GSJ core penetrating the Nojima Fault, Awaji Island, Southwest Japan, The Journal of the Geological Society of Japan, 150, 72-85

Tsukamoto S. and Iwata S. (2005) Recent development in luminescence dating; on the extending the age range and the behavior of different OSL components from quartz, The Journal of the Geology Society of Japan, 111, 643-653

Toyoda S. and Ikeya M. (1991) Thermal basis stabilities of paramagnetic defect and impurity centers in quartz: Ba-sis for ESR dating of thermal history, Geochemical Journal, 25, 437-445

Watanabe Y. Nakai S. and Lin, A. (2008) Attempt to determine U-Th dating of calcite veins in the Nojima fault zone, Japan. Geochemical Journal, 42, 507-513

Wintle A.G. and Murray A.S. (2006) A review of quartz optically stimulated luminescence characteristics andtheir relevance in single-aliquot regeneration dating protocols, Radiation Measurements, 41, 369-391

Yamada R. Matsuda T. and Omura K. (2007) Apatite and zircon fissiontrack dating from the Hirabayashi-NIED borehole, Nojima Fault, Japan: Evidence for anomalous heating in fracture zones. Tectonophysics, 443, 153-160.

Zwingmann H. Yamada K. and Tagami T. (2010) Timing of brittle deformation within the Nojima fault zone, Japan, Chemical Geology, 275, 176-185

CHAPTER 3

3. Optically stimulated luminescence signal resetting of quartz gouge during subseismic to seismic frictional sliding

3.1 Introduction

Determining the timing of the most recent faulting event and the recurrence intervals of Quaternary faults is crucial for understanding the tectonics of active continental margins and for assessing seismic hazard. Paleoseismological approaches to assessing recent fault activity are mainly based on cross-cutting relationships between faults and overlying near-surface Quaternary sediments. However, this approach is not applicable to faults that are not accompanied by Quaternary sediments, or where the sediments lack datable materials (e.g. peat). In addition, the lack of young sediments precludes the application of this method to faults at depth (e.g., a fault zone recognised by drilling). Other attempts to determine the age of fault rocks have been made using (1) radiometric dating techniques such as K-Ar (e.g. Kralik et al., 1987; Zwingmann & Mancktelow, 2004), (U-Th)/He (e.g. Wölfler et al, 2010) and fission-track (FT) methods (e.g. Murakami & Tagami, 2004; Yamada et al., 2007) and (2) the trapped-charge dating techniques such as electron spin resonance (ESR) (e.g. Fukuchi, 1996; Ikeya et al., 1982) and luminescence (e.g. Banerjee et al., 1999). These methods are based on the concept that age resetting of pre-existing minerals occurs during heating induced by high-velocity fault slip (e.g. (U-Th)/He and FT dating of zircon/apatite and ESR and luminescence dating of quartz) or synkinematic crystallization occurs due to hydrothermal fluid flow associated with fault rupture (e.g. K-Ar dating of authigenic illite). Among these methods, K-Ar, (U-Th)/He, FT and ESR methods have an effective dating range from 10,000 years to more than 1 million years ago (~0.1 Ma to a few Ga for K-Ar, ~1 to 100 Ma for (U-Th)/He, ~0.1 to 100 Ma for FT, and 10,000 years to ~1 Ma for ESR) due to their long half-lives, making them inadequate for dating the most recent event of active Quaternary faults (≤1,000 years). In addition, the relatively high closure temperature of K-Ar, (U-Th)/He and FT methods may preclude complete age resetting during short-lived frictional heating in the subsurface environment (Tsukamoto et al., 2020).

Optically stimulated luminescence (OSL) and thermoluminescence (TL) dating methods rely on the increase in the trapped charge population in a target crystal due to its exposure to environmental radiation (e.g., Smedley, 2018). The amount of trapped charge, which is proportional to the time elapsed since the onset of charge storage, can be estimated as a form of luminescence by artificial exposure to light (OSL) or heat (TL) in a laboratory. The luminescence signal profile varies between samples (e.g. fast component dominant or slow component dominant for OSL), reflecting the type of traps they have. These methods have two characteristics that make them suitable for dating Quaternary faults, namely (1) an effective dating range of a few decades to a few million years (Smedley, 2018) and (2) a high sensitivity to heat due to the ultralow closure temperature (Guralnik et al., 2013). An early study of luminescence dating of fault material successfully determined the age of the last seismic

event on a Quaternary fault in central Japan (Ganzawa et al., 2013). Their study also showed that the fast component of the quartz OSL signal, which is suitable for dating (Singarayer & Bailey, 2003; Wintle & Murray, 2006), loses intensity rapidly (<20 s) at a temperature of 300°C under static heating. Recently, much attention has been paid to friction experiments designed to demonstrate co-seismic age resetting of OSL and TL. Yang et al. (2019) conducted high-speed friction experiments on dry quartz gouges at slip rates on the order of metres per second, and found a clear reduction in OSL and TL signals in recovered samples. Kim et al. (2019) conducted high-velocity friction experiments for dry quartz-clay mixed gouges and reported the absence of OSL in recovered quartz grains. These studies also confirmed that the luminescence intensity does not decrease in experiments with slow slip rates (0.06, 0.002 and 0.001 ms^{-1}). However, the dependence of signal loss on the slip rate applied to such samples has only been studied at limited slip rates (millimetres per second and metres per second), and therefore the relationships between OSL signal reduction, slip rate and frictional heat generated in the samples by aseismic to seismic slip rates remain unclear.

Another issue that needs to be explored is the potential application of granite-derived quartz to assess Quaternary fault activity. In their experiments, Yang et al. (2019) and Kim et al. (2019) used sediment-derived quartz (sand), which generally has a fast OSL component. In contrast, those from fresh metamorphic or plutonic rocks are considered unsuitable for dating due to significant contributions of non-fast (medium and slow) OSL components, insensitivity of the fast OSL component, and potential signal contamination by feldspar (Guralnik et al., 2015; Jeong & Choi, 2012). Since basement rocks of continental (arc) crust are commonly composed of granite, Quaternary faults in active continental margins do not always accompany sediments, but are often surrounded by granite. Therefore, although the OSL of granite-derived quartz cannot provide a reliable age, it should provide useful information by semi-quantitatively assessing recent fault activity in cases where a co-seismic signal reduction is detected. For example, if the OSL signal in the fault zone is not saturated while that of the surrounding rock is, we can say that the fault zone must have experienced thermal events to reduce the OSL intensity in the last ~200 ka (the time typically required for saturation of quartz OSL). Based on the above research background, we extend the work of Kim et al. (2019) and Yang et al. (2019) by performing friction experiments on granite-derived quartz over a range of 4 orders of magnitude in slip rate (0.0002 to 1.3 m s^{-1}) and establish an empirical relationship between OSL signal reduction and fault slip rate. We then estimate the seismological and geological conditions required to reset OSL ages in natural fault zones. Finally, we demonstrate the potential applicability of granite-derived quartz for Quaternary fault detection and evaluation.

3.2 Materials and Methods
3.2.1 Starting Materials

The quartz used in this study was extracted from the Tsushigawa granite collected along the

Nojima branch fault at the Ogura trench site (Nishiwaki & Lin, 2019, Figure 3-1(a)), located in northern Awaji Island, western Japan. The Nojima branch fault is known to have ruptured during the 1995 Hyogoken Nanbu earthquake. The granite sample (Figure 3-1. (b)) was taken from the eastern wall of the trench, ~6 m from the fault core. The sample was crushed in a mortar and then magnetic minerals and other impurities (coloured minerals) were removed using a magnet and tweezers. The crushed sample was treated with 23% HF for 100 min and 18% HCl for 24 h to remove feldspars and clay minerals. Although the sample after HF treatment contained a small amount of feldspar, we decided to retain this combination of concentration and reaction time (23% HF, 100 min), as a higher concentration and/or longer reaction time may cause damage to the mineral surface (further details of the purification process are described in Section 2.3).After acid treatment, the quartz grains were dried and sieved to obtain a grain size of <150 μm (Figure 3-1(c)). These preparations were made under sunlight or fluorescent light. Although the natural signal should have been optically bleached (erased) by the light, the grains were further heated to 300°C for 2 h prior to laboratory irradiation to ensure the absence of trapped electrons. The grains were then wrapped in aluminium foil to avoid exposure to light and irradiated with gamma rays using the 60Co gamma ray irradiation facility at the Institute for Integrated Radiation and Nuclear Science, Kyoto University, Kyoto, Japan, to cause the specified radiation damage to the sample.

3.2.2 Friction Experiments

Friction experiments were performed using a rotary shear high-speed friction apparatus at Yamaguchi University, Yamaguchi, Japan (Figure 3-2(a); Hirose & Shimamoto, 2005). For all friction experiments, gamma-irradiated quartz grains (1 g) were placed between two gabbro cylinders with a diameter of 25.0 mm (Figure 3-2(b); for details see Oohashi et al., 2013). All experiments were performed under dry conditions, except for one experiment (HVR4237), which was performed in 0.5 ml of distilled water. In all experiments, a K-type thermocouple was placed on the stationary side of the host rock to measure the temperature of the fault zone during shearing. The tip of the thermocouple closest to the sliding surface (TC1) was placed 2.5 mm from the circumference of the cylinder and exposed to the sliding surface. The other two thermocouples (TC2 and 3) were buried ~3 and 5 mm below the surface respectively. A Teflon sleeve with an internal diameter of 24.95 mm was placed around the simulated fault zone to prevent leakage from the gouge.

After mounting the specimen assembly in the apparatus, a normal stress (σ_n) of 1.0 MPa was applied. Experiments were conducted at equivalent slip rates (V_e) from 0.0002 m s^{-1} (200 μm s^{-1}) to 1.3 m s^{-1}, constant normal stress of 1.0 MPa and constant displacement (d) of ~10 m (Table 3-1). Since the slip rate increases from the centre to the periphery of the cylindrical sample, we use the equivalent slip rate (V_e), which is defined such that $\tau V_e S$ gives the rate of total frictional work on a fault with an area of S, assuming a constant shear stress (τ) across the fault surface (Shimamoto & Tsutsumi, 1994).

For convenience, we refer to the equivalent slip rate as the slip rate or velocity (V). Normal stress and shear stress were calculated from the recorded normal force and torque using the known area of the fault surface (0.00049 m^2) and the assumption that the shear stress is constant over the fault surface regardless of the variation in slip rate over the surface. We report the coefficient of friction (μ) in terms of the measured shear stress normalised to the measured normal stress ($\mu = \tau/\sigma_n$). In addition to the friction experiments for OSL measurements, we also performed high speed friction experiments for microtextural observations.

After the experiments, deformed samples were collected for OSL measurements. Since slip rate and displacement are zero at the centre and maximum at the periphery, samples were taken from annular regions 0-3 (or 2-3) mm from the periphery of the circular shear plane (Figure 3-2(c)) to avoid slip rate and displacement heterogeneities. We refer to the equivalent slip rate and displacement of this zone as V_{sp} and d_{sp}, respectively. The recovered samples were sieved to obtain coarse grains (75-150 μm) and to minimise the effect of crushing on the OSL signals. All procedures after gamma irradiation were performed in a darkroom environment to avoid resetting of the OSL signal due to exposure to light.

3.2.3 OSL measurement

Samples before and after the friction experiments were analysed using an OSL reader (Medec, Hakodate, Japan; for details, see Ganzawa et al., 2013) installed at Kanazawa University, Kanazawa, Japan. The OSL reader is equipped with blue LED light sources (λ = 470 nm; 75 mW cm^{-2}), a photomultiplier tube (R585s; Hamamatsu Photonics, Hamamatsu, Japan) sensitive to blue to violet light, a UV band-pass filter (RR0340; Asahi Spectra, Tokyo, Japan), and an X-ray source (VF-50; Varian Medical Systems, Palo Alto, USA; dose rate = 6.0 Gy [Gray] min^{-1}; Hashimoto & Nakagawa, 2002). A single aliquot regenerative dose (SAR) protocol (Murray & Wintle, 2000; Wintle & Murray, 2006, Table 3-2) was used, in which a measurement after the administration of a constant dose (referred to as the test dose) is intercalated between the main measurement to track the change in sensitivity of the material being measured. Each aliquot (sample disc) is first 'pre-heated' (220°C, 10 s) to remove unstable components of the OSL signal (see Table 3-2). Then the blue LED light is emitted at 125°C for 60 s to stimulate the OSL of the quartz grains ("main measurement"). The OSL signal of the measurement is detected and measured by a photomultiplier tube. The main measurement is followed by the irradiation of the test dose (10 Gy) and the OSL signal is measured again ("test measurement") to normalise the sensitivity difference between the aliquots. A "cut heat" (180°C, 10 s) is applied between the irradiation and the test measurement to eliminate unstable components induced by the test dose. The net OSL signal intensities of the main and test measurements (Ln and Tn, respectively) are derived from the initial OSL signal (1 s) minus a background estimated from the last 1 s of stimulation. To determine the appropriate preheat temperature, we performed preheat dose

recovery tests prior to measurements (Figure 3-3). We measured 5-20 aliquots of 20 coarse quartz grains for each sample. As a small amount of feldspar, recognisable by its milky white colour, was identified in the starting material, we carefully hand-picked transparent quartz grains using a light microscope and fine brushes in a darkroom environment.

3.2.4 Determination of OSL measurement conditions

The experimental results necessary to decide the preheat temperature in the measurement protocol is shown in this subsection. Five quartz aliquots are prepared and 100 Gy was given by the in house X-ray source after removing the potential remining dose by the hot bleach at 280°C for 40 seconds. Then the conventional SAR protocol (Murray and Wintle, 2000) with various preheat temperatures (180-260°C with 20°C interval) was applied to measure the equivalent dose. Cut heat temperature was set as preheat temperature minus 40°C (140-220°C). The measurement protocol is given in Table 3-3. Instrumental setting is the same with the description above. Because of no significant dependence of data on preheat temperatures in the applied temperature range (Figure 3-3 and 3-4), we accepted the conventional preheat condition of 220°C for 10 seconds. Linearly modulated luminescence (LM-OSL, Bulur, 1996, Jain et al., 2003) was also measured after preheating at various temperatures (180-260°C with 20°C interval).LM-OSL is a technique for measuring the OSL signal while increasing the intensity of the excitation light from zero at a constant rate. Using this method, the OSL signal of quartz can be separated into up to seven components (ultra fast, fast, medium, slow 1-4) (Tukamoto et al., 2005).

LM-OSL curve deconvolutions were made assuming a linear combination of more than one first-order components, each defined by

$$L = Ab(t/P)exp(-bt^2/2P)$$

where A is the amplitude proportional to trap population n_0, b is detrapping probability proportional to photo ionisationcross-sectionσ and maximum light intensity I_0 ($b=\sigma I_0$) and P is the total observation time (Bulur, 1996; Jain et al., 2003).

LM-OSL results (Figure 3-5) also indicate this preheat setting is reasonable for majority of samples to obtain significant intensity of signal with less disturbance from the unstable signal.

3.3 Result

3.3.1 Friction Experiments

At relatively low slip rates of 0.0002 to 0.01 ms^{-1}, the coefficient of friction is 0.55-0.80 immediately after the start of the experiments and has a broadly constant value or shows a slight increase in slip throughout the experiments (Figure 3-6(a)). For this range of slip rates, the temperature of the sliding surface shows no significant increase (≤53°C) during slip (Figure 3-6(c) and Table 3-1). In contrast, the sheared experiments at V ≥ 0.06 m s^{-1} show a slip-weakening behaviour after a peak

friction of 0.65-0.80 and a decrease towards a friction of 0.4-0.5 (with the exception of hvr4233; Figure 3-6(b)). A significant decrease in friction, characterised by an initial peak friction followed by an exponential decay towards a steady-state friction ($\mu_{ss} \sim 0.2 \pm 0.1$ in many cases) over a slip-weakening distance, is widely recognised in high-velocity friction experiments for both intact rocks and incohesive gouges (e.g. Di Toro et al., 2011; Mizoguchi et al., 2009). However, we could not find a clear steady state in our experiments conducted at $V = 0.4\text{-}1.3 \text{ m s}^{-1}$. This can be explained by the fact that the applied displacement (10 m) is shorter than the slip weakening distance of quartz gouge ($\sim$15 m under σ_n of 1 MPa and $V = 1 \text{ m s}^{-1}$; Togo & Shimamoto, 2012), and therefore the experiments were stopped before the friction reached a steady state. The maximum temperature measured during the experiments increases from ~90°C to 270°C with increasing slip rate (Figures 3-6(c) and 3-6(d)). The sample with water added and sheared at $V = 1.3 \text{ m s}^{-1}$ (hvr4237) also experienced a temperature of >190°C during the experiment.

3.3.2 OSL measurement

The starting material OSL signal was measured for the gamma irradiated quartz grains without the application of normal stress and shear deformation. Although the OSL decay curves of the starting material measured by continuous wave OSL (CW-OSL) show variability in intensity between the aliquots (Figure 3-7(a)), they show sharp peaks in the first second of stimulation, which decrease rapidly in the following seconds. The sensitivity-corrected OSL signal (Ln/Tn; luminescence intensity normalised to the test dose of 10 Gy) is characterised by a wide range of values from 0.5 to 7.0 (mean Ln/Tn = 3.15 ± 1.66; equivalent dose De = 31.5 ± 16.6 Gy), which may be due to variations in the luminescence properties of the granite-derived quartz grains. The shapes of the LM-OSL show that the signal consists of a high to medium fast component, a medium slow component and a low slow component (Figure 3-5).

The OSL decay curves of the recovered samples sheared at $V = 0.0002$ to 0.13 m s^{-1} are similar to those obtained with the starting material (Figures 3-5 and 3-7(a)). The mean Ln/Tn values of these samples vary from 0.62 to 2.31 (mean 1.72 ± 0.71), which are not significantly different from the starting material (Figures 3-9 and 3-10(a)). In contrast, the OSL intensities of the samples sheared at $V \geq 0.25 \text{ m s}^{-1}$ have no visible peaks after stimulation (Figure 3-8). The Ln/Tn value is <1 for all these aliquots and the mean Ln/Tn and standard deviation (error) values decrease with increasing slip rate (Figure 3-8). It should be noted that the Ln/Tn values of the starting material are in all cases >0.5 (Figure 3-7(b)) and there is a clear difference (beyond the margin of error) in luminescence intensity between the starting material and the samples obtained from the high speed friction experiments. Furthermore, at $V = 0.25$ and 0.40 m s^{-1}, histograms of Ln/Tn values show scattered or multimodal distributions (ranging from ~0.1 to 1), indicating that the luminescence signals of only part of the grains in a sample were zeroed during the experiments (Figure 3-9). On the other hand, those of

samples sheared at $V \geq 0.65$ m s^{-1} show a unimodal distribution with a mean Ln/Tn value close to zero (≤ 0.1), indicating that almost all grains in a sample lost signals (hereafter referred to as 'partial resetting' and 'complete resetting' for the former and latter cases, following the definition used in luminescence dating; Smedley, 2018). Notably, the water-added sample sheared at $V = 1.3$ m s^{-1} also shows resetting of the OSL signal during the friction experiment. The OSL intensities (mean Ln/Tn) of the recovered samples show a clear relationship with the applied slip rate. At $V_{sp} = 0.0003$ to 0.18 m s^{-1}, Ln/Tn has an almost constant value of 1-2 (Figure 3-10(a)). At $V_{sp} \geq 0.33$ m s^{-1}, Ln/Tn decreases exponentially from 101 to 10-2 towards a co-seismic slip rate of 1 m s^{-1}.

3.3.3 Temperature Estimation Within the Gouge Zone

The temperature directly measured by thermocouple TC1 during the experiments is the temperature at the boundary between the gouge zone and the stationary side of the cylinder (Figure 3-2 (b)). However, slip is often localised at the boundary between the rotating side of the cylinder and the gouge zone (e.g. Kitajima et al., 2010; Yao et al., 2013). Thin section observations confirm that a slip-localised zone of 80-100 μm thickness was formed adjacent to the rotational side of the cylinder (Figure 3-11(a)). As the thermocouple was placed ~1.2mm from the heat source (slip-localised zone), the maximum temperature in the gouge zone cannot be measured directly. Therefore, we estimate the maximum temperature within the gouge zone (slip-localized zone) during the experiment using COMSOL Multiphysics, a commercial finite element modeling software, following the procedures of Kitajima et al. (2010) (Figures 3-11(b) and 3-11(c)). The exact buried positions (i.e. depths) of the thermocouples were measured by X-ray CT after recovery of the gouge sample. The results of the calculation show a large temperature difference along the gouge zone, with a minimum at the centre of the gouge and a maximum at the periphery of the gouge (Figure 3-11(c)). However, the temperature in the region from which we took samples for OSL measurements (outermost 3 mm) was almost uniform. A large temperature gradient was observed across the gouge zone, even in a gouge zone of ~1.2 mm thickness. For example, at $V = 1.3$ m s^{-1}, the temperature was 494°C in the gouge zone and ≤ 250°C on the other side of the zone (Figure 3-11(c)). We assume that the maximum calculated and measured temperatures are the upper and lower limits, respectively, of the temperature to which the specimen was subjected during an experiment. As V increases from 0.13 to 1.3 m s^{-1}, the maximum calculated temperature increases from 150°C to 500°C, while the maximum measured temperature increases only from 120°C to 180-270°C (Figure 3-10 and Table 3-2).

3.4 Discussion
3.4.1 Mechanism of OSL Signal Resetting During Friction Experiments

Our results show that the OSL signal decreases dramatically during high velocity friction experiments. Previous studies have shown that the TL and OSL intensities of quartz grains decrease

(or locally become zero) after slow slip rate experiments (V = 16 to 56 μms^{-1}) (Bateman et al., 2018; Hiraga et al., 2004). Hiraga et al. (2004) find an inverse relationship between TL intensity and applied frictional work. However, the frictional work per unit area, WF, in the experiments of the present study is almost constant (5.9 ± 0.9 MJ m^{-2}; Table 3-1) and shows no relationship with V. Therefore, the observed OSL resetting cannot be attributed solely to frictional work.

It is generally accepted that the OSL signal decreases with increasing temperature and heating time and the OSL lifetime can be expressed on an Arrhenius plot (Aitken, 1985; Murray & Wintle, 1999). In the gouge zone of the sample sheared at V = 1.3 m s^{-1}, temperatures ranged from 181-272°C (lower limit) to 500°C (upper limit) (Table 3-2 and Figure 3-10), which are high enough to cause thermal annealing of the OSL signal in less than a few minutes (Jain et al., 2003; Murray & Wintle, 1999; Singarayer & Bailey, 2003). Ganzawa et al. (2013) found that only 10-20 s of heating is required to reduce the initial OSL component, based on annealing experiments at a fixed temperature of 300°C. Since the duration of our high-speed friction experiments (8-15 s) was comparable to that of Ganzawa et al. (2013), the observed OSL resetting during our experiments can be attributed to frictional heating. On the other hand, samples sheared at V = 0.25 and 0.40 m s^{-1} did not experience resetting, even though the OSL intensities were significantly lower than in the starting material. The temperatures within the gouge zones were estimated to be 240°C for the slip-localised zone and 150°C for the less deformed zone (Table 3-2 and Figure 3-11). In this temperature range, the OSL signal must be zero or significantly reduced in the slip-localised zone, but remains unchanged in the less deformed zone. We interpret this partial reset as being due to the heterogeneous temperature conditions within the gouge zones.

The observed resetting of the OSL signal can primarily be explained by thermal annealing due to frictional heating. However, resetting also occurs at temperatures lower than expected from static heating tests. For example, the lower temperature limit of the gouge zones sheared at V = 1.3 m s^{-1} in some experiments (hvr4235 and 4237) was only 180-190°C, and the temperature required for complete OSL resetting in an 8 s duration is estimated to be 320-340°C (Murray & Wintle, 1999; Singarayer & Bailey, 2003). Short-term static heating tests (Ganzawa et al., 2013; Kim et al., 2019) are also consistent with this estimate. Further research is needed to understand the details of OSL signal decay during high velocity friction experiments (i.e., effects of friction and/or fracture, Hiraga et al., 2002, 2004; effects of stress concentration, Bateman et al., 2018; and effects of thermal annealing on short-lived static heating of the starting material).

3.4.2 Power Density and Depths Required for OSL Resetting

The frictional work rate is the key parameter for understanding thermally activated processes during high-velocity friction, as the heat generated by a large amount of frictional work is buffered in a small volume of rock, resulting in a high temperature in the slip zone. Di Toro et al. (2011) introduced

the power density term (frictional work rate; $\tau_e V$), which is proportional to both the equivalent shear stress (τ_e) and the slip rate. Since the equivalent shear stress requires the steady-state shear stress for the calculation, and the friction of our high-speed experiments did not reach steady state, we used the equation proposed by Aretusini et al. (2017) (the frictional work divided by the duration of the experiment) to obtain the power density (Table 3-1). The power densities of our friction experiments show a clear relationship with the measured/calculated temperatures and OSL intensities (Figure 3-10(b)). Partial and complete resetting of the OSL signal occurs when the power density exceeds 0.17 and 0.6 MW m^{-2} respectively.

Since the shear stress is proportional to the normal stress in Coulomb's friction law ($\tau = \mu\sigma_n$), the power density is also proportional to the normal stress. Using this relationship, the effective normal stress required to reset the OSL can be estimated. Assuming a co-seismic slip rate of 0.6 m s^{-1} from the slip inversion of an earthquake (e.g. 1995 Hyogoken Nanbu earthquake; Ide & Takeo, 1997), τ_e for partial and complete OSL resetting are 0.28 and 1.0 MPa, respectively. The friction law gives normal stresses of 0.47 and 1.67 MPa when dynamic friction can be approximated as 0.6 (see Figure 3-5(b)). Assuming an angle between a fault plane and a maximum principal stress σ1 of 30°, a rock friction of 0.6 and no pore pressure, the Mohr-Coulomb failure criterion gives σ1 and the minimum principal stress σ3 of 0.97 and 0.30 MPa respectively for partial settling and 3.70 and 1.09 MPa respectively for complete settling. Since σ1 or σ3 is equal to the overburden pressure σ_z (which is the lithostatic pressure at depth z) for normal and reverse faults, the partial and complete resetting depths can be estimated to be 37 and 133 m for normal faults and 11 and 42 m for reverse faults (assuming a rock density of 2.65 g cm^{-3} and a gravity acceleration of 9.806 m s^{-2}). These estimates may be a lower bound (shallowest case) for the depth of co-seismic OSL resetting, as the dynamic friction at higher normal stress (>1.0 MPa) becomes a smaller value (<0.6) due to the short slip weakening distance and low μss (Togo & Shimamoto, 2012). In addition, the presence of clay minerals in fault gouges may lead to a low coefficient of friction and consequently require higher normal stress (much deeper depths) for resetting. Nevertheless, our result implies that co-seismic OSL resetting of quartz-rich faults occurs in the near-surface environment of the Earth's crust. In practice, samples need to be taken from depths greater than a few tens to a few hundred metres by digging a trench, borehole or tunnel to make a good estimate of the timing of the last co-seismic event.

3.5 Conclusions

1. To understand the dependence of OSL signal reduction on fault slip rate, we performed friction experiments on a granite-derived quartz gouge at various slip rates ($V = 0.0002$ to 1.3 m s^{-1}), normal stress of 1.0 MPa and displacement of 10 m. The normalised OSL intensity (Ln/Tn) after the dry friction experiments starts to decrease from $V = 0.25$ m s^{-1} ($V_{sp} = 0.34$ m s^{-1}) and becomes zero at $V \geq 0.65$ m s^{-1} ($V_{sp} \geq 0.8$ m s^{-1}). Partial reset occurs at $V = 0.25$ and 0.40 m s^{-1} ($V_{sp} = 0.34$

and 0.53 m s^{-1}). Reset of the OSL signal also occurs in the water-added experiment sheared at V = 1.3 m s^{-1}.

2. A clear inverse correlation is observed between the measured/calculated temperatures of the gouge zones and the OSL signal intensities. Partial resetting occurs when the maximum temperature within the gouge zone reaches ~240°C, whereas complete resetting occurs when the minimum temperature satisfies 181-271°C. Given that thermal annealing of the OSL signal at 300°C takes several tens of seconds, the observed OSL signal decay (resetting) can be primarily explained by frictional heating.

3. OSL signal intensities decrease exponentially with increasing power density, which is a function of heat generation during high-speed friction. The power densities required for partial and complete OSL resetting are ≥0.17 and ≥0.6 MW m^{-2}, respectively. Assuming a co-seismic fault slip rate of 0.6 m s^{-1}, the depth conditions required for partial and complete OSL resetting are expected to be ≥11 and ≥42 m, respectively.
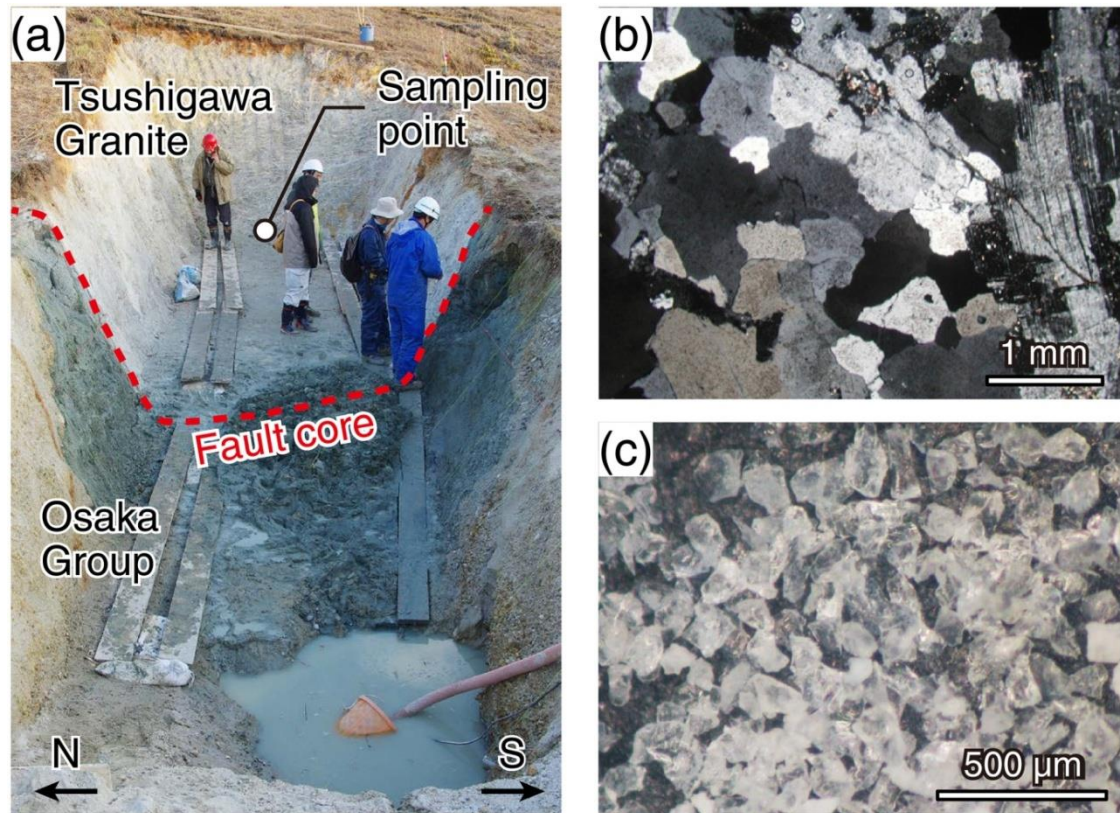
Figure 3-1.(a) Photograph showing the Nojima branch fault, Ogura trench, which was excavated in 2015. Weakly sheared Tsushigawa Granite from the east wall of the trench was taken for starting material. (b) Photomicrograph (cross-polarized light) of the granite. (c) Purified quartz grains (<150 μm) used for the friction experiments.
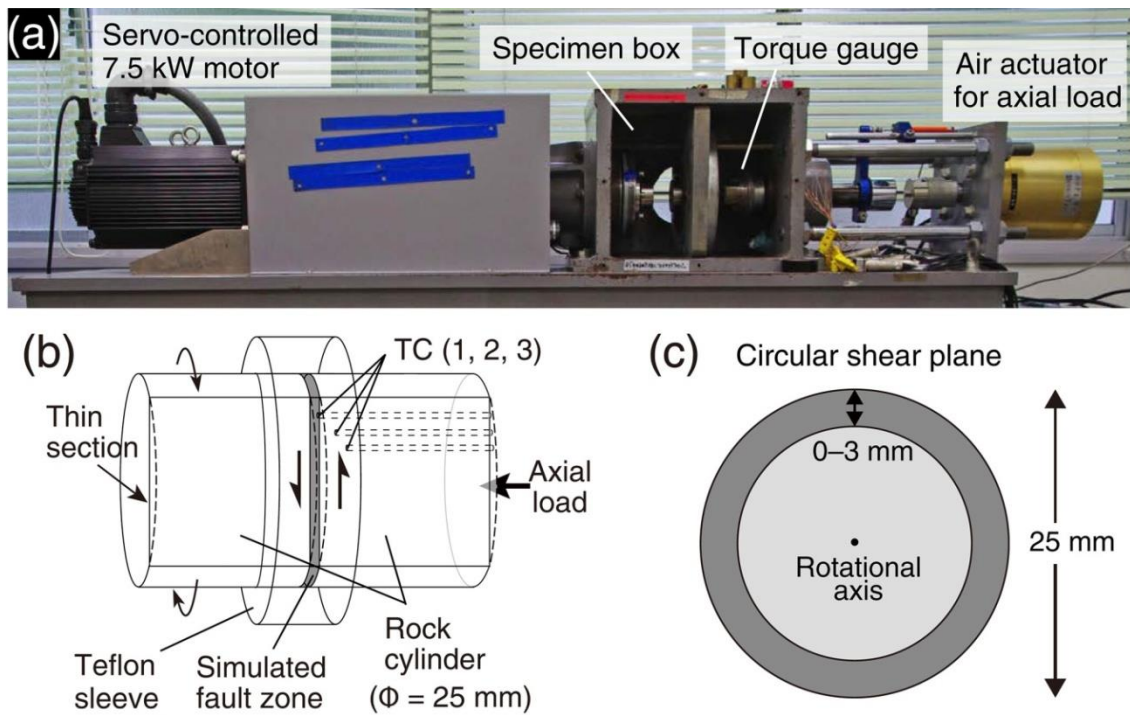
Figure 3-2.(a) Rotary-shear, high-velocity friction apparatus at Yamaguchi University. (b) Specimen configuration used in this study. Simulated fault gouge was placed between two cylinders of gabbro. Temperature was measured using three K-type thermocouples (TC1, 2, and 3; buried at different depths) placed 2.5 mm inward from the circumference ofthe cylinder. (c) Schematic illustration showing the circular shear plane of the simulated fault gouge. The sampler covered from the annulus region (0–3 mm) was used for OSL measurement.
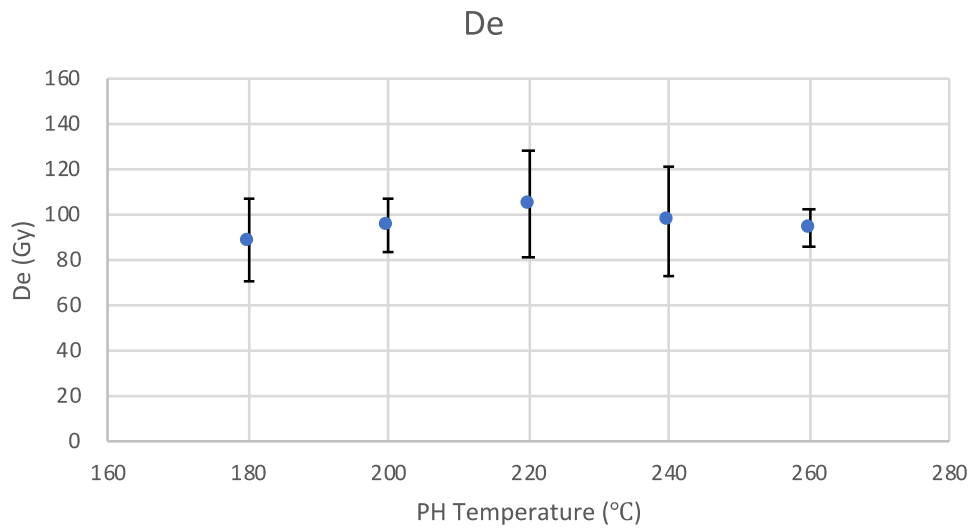
Figure 3-3. Results of equivalent dose measurement plotted against preheat temperatures.   Averages of five measurements are plotted with one sigma standard deviation.   All preheat conditions show data which overlap 100 Gy.
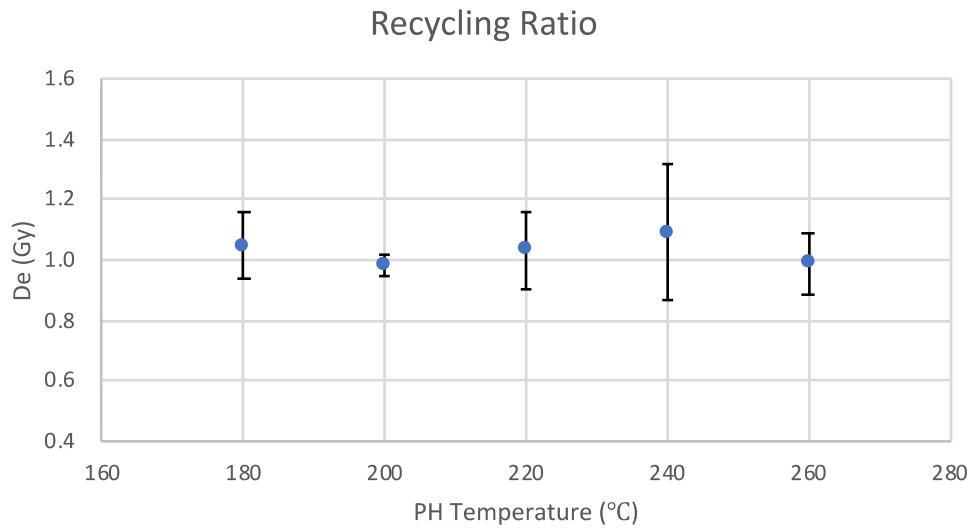
Figure 3-4. Results of recycling ratio plotted against preheat temperatures.   Recycling ratio is calculated by estimating the equivalent dose of the last 50 Gy irradiation. Averages of five measurements are plotted with one sigma standard deviation.   All preheat conditions show data around unity.
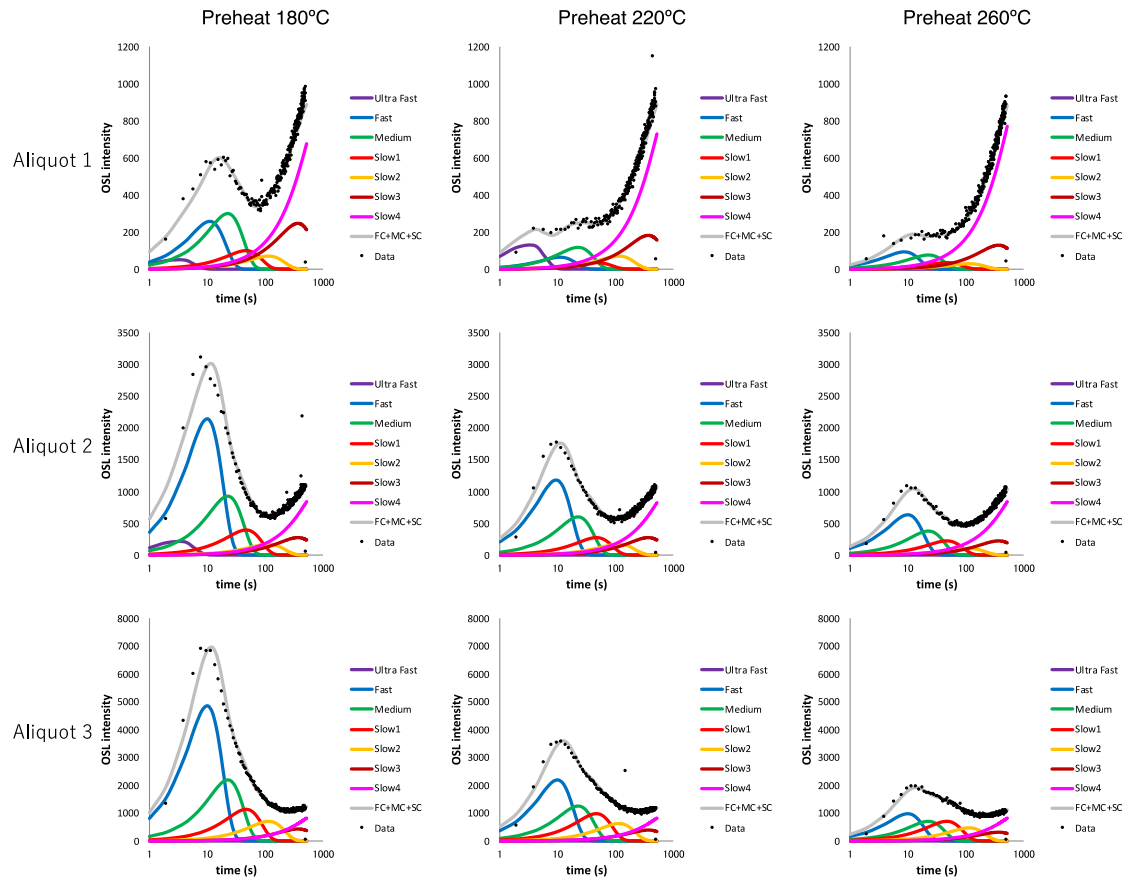
Figure 3-5. Results of lineally modulated OSL (LM-OSL) measurement for representative three aliquots to identify signal components. Two other aliquots are similar with aliquot-3. Few samples seem to keep unstable ultrafast signal after the preheat at 220°C (aliquot-1), but majority of samples do not have the ultrafast component (aliquot-3). Ultrafast component for one sample (aliquot-2) was deleted by the preheating at 220°C and more. Signal intensities are decreased when preheat temperature is high.
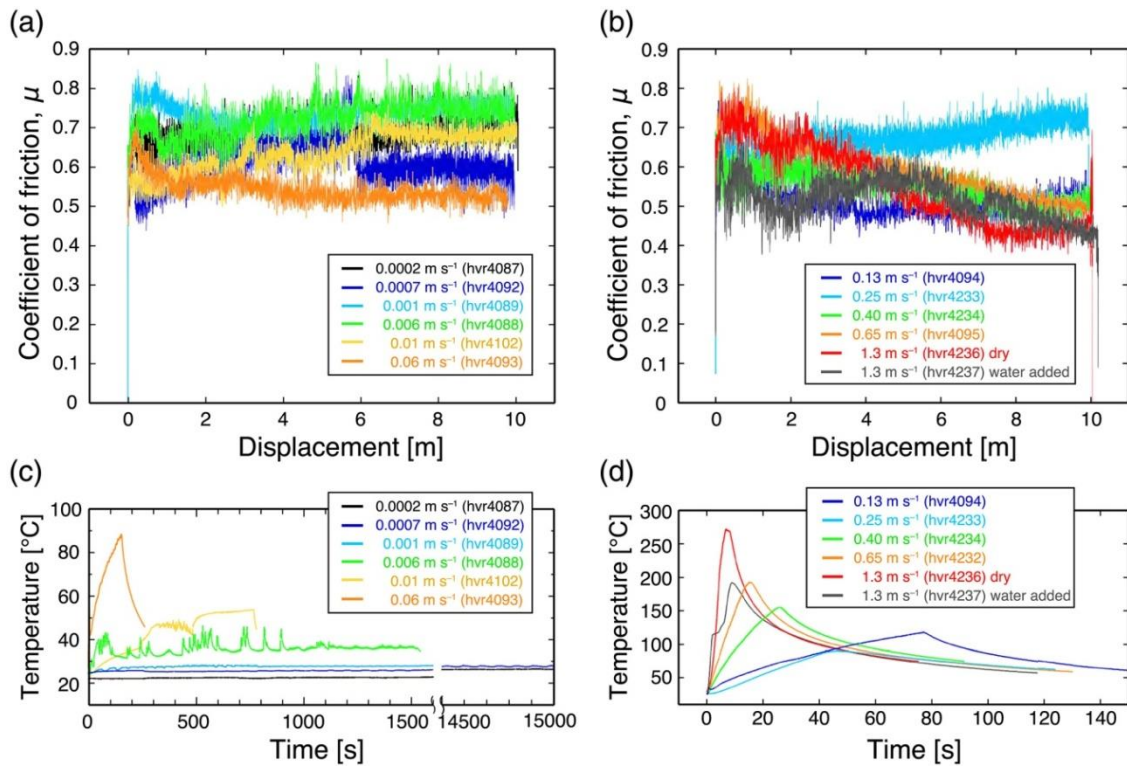
Figure 3-6.Mechanical behavior of quartz gouges at (a) low slip rates (V) of 0.0002–0.006 m s^{-1} and (b) high V of

0.13–1.3 m s^{-1}. (c) and (d) show temperatures measured by TC1 during each experiment.
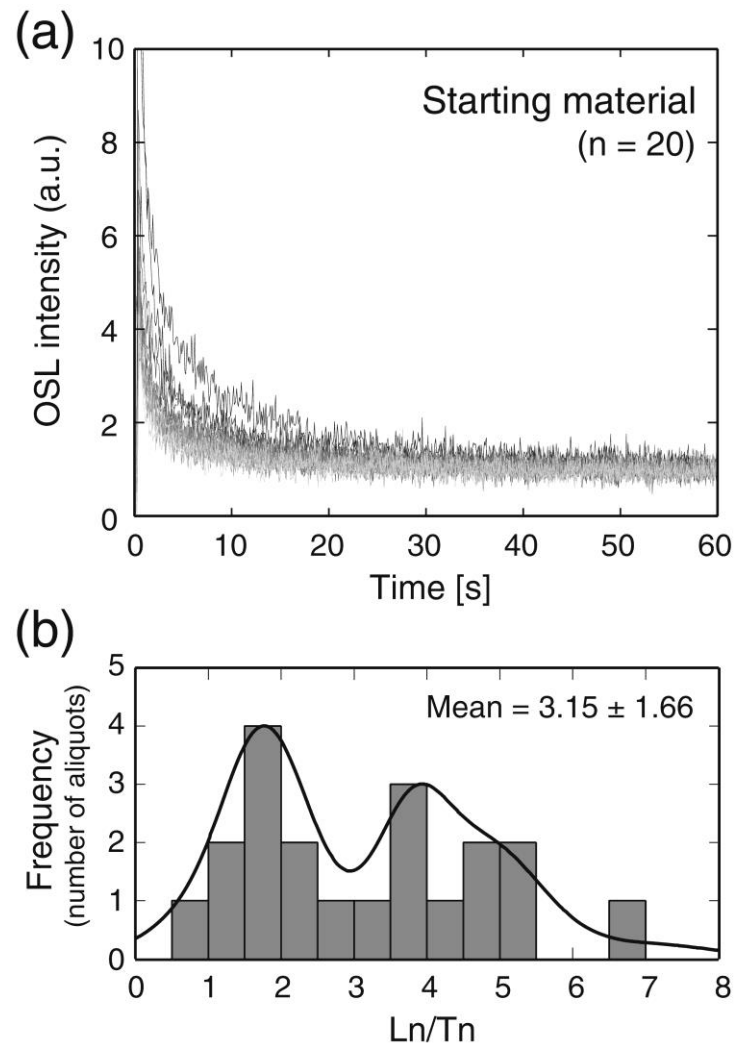
Figure 3-7. Results of OSL measurements on the starting material. (a) CW(continuous wave)-OSL decay curves stimulated with blue LED light (75mWcm^{-2}) at 125°C following a 220°C preheat for 10 s. (b) Histogram ofthe sensitivity-corrected OSL signal (Ln/Tn; luminescence intensity normalized to the test dose of 10 Gy). A total of 20 aliquots each containing 20 grains of quartz was measured.
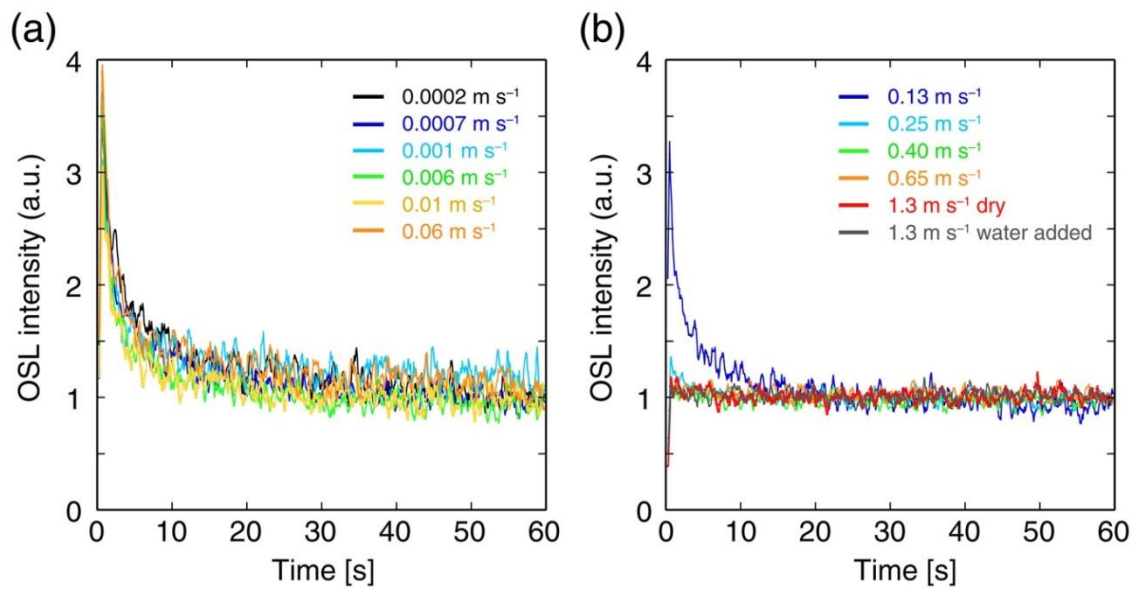
Figure 3-8. OSL decay curves of recovered samples sheared at (a) $V = 0.0002$–0.06 m s^{-1} and (b) $V = 0.13$–1.3 m s^{-1}.
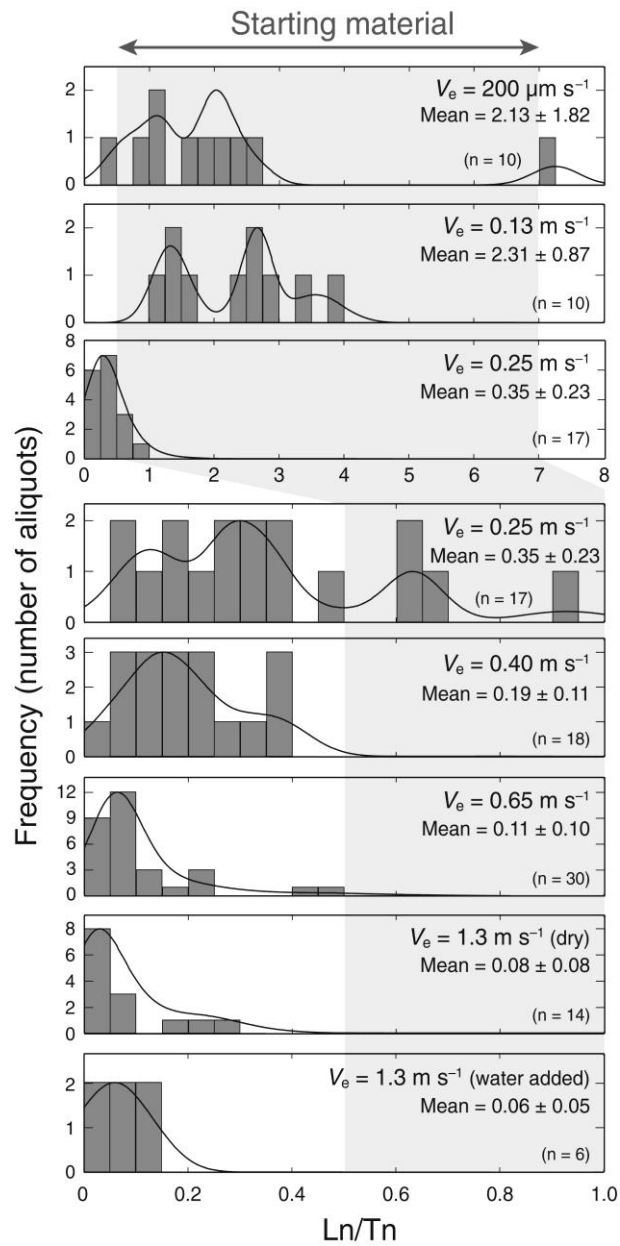
Figure 3-9.Histograms with kernel density estimates (KDE) of Ln/Tn for samples recovered after the friction experiment. Note that horizontal axes for the upper three diagrams range from 0 to 8, whereas those for the lower five diagrams range from 0 to 1. Double arrow and shaded area indicate the range of Ln/Tn observed in the starting material. Error is derived from the standard deviation (1σ) of measurements. KDE plots were generated using Density Plotter 8.5 from Vermeesch (2012).
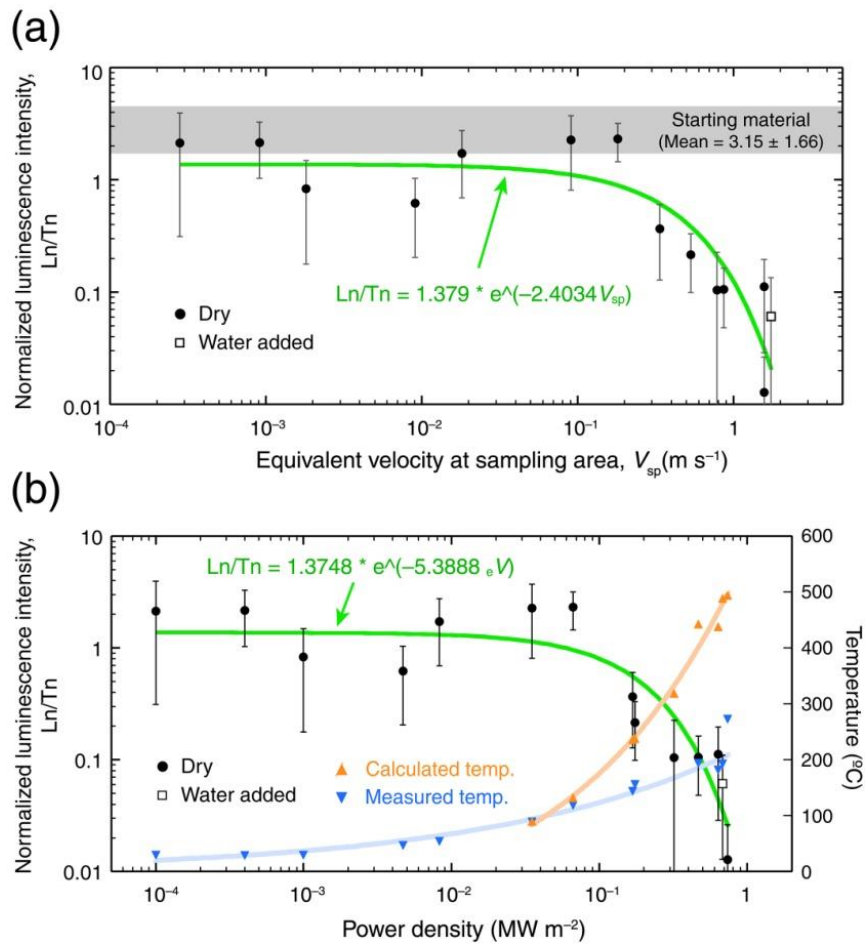
Figure 3-10. (a) Ln/Tn plotted versus equivalent velocity at sampling area (V_{sp}). The green curve is a least squares fit with an exponential function. (b) Measured (TC1) and calculated (FEM) temperatures plotted together with Ln/Tn against power density ($\tau_e V$). Blue and orange curves are least squares fit to the temperatures with a power law. Error is derived from the standard deviation (1σ) of measurements.
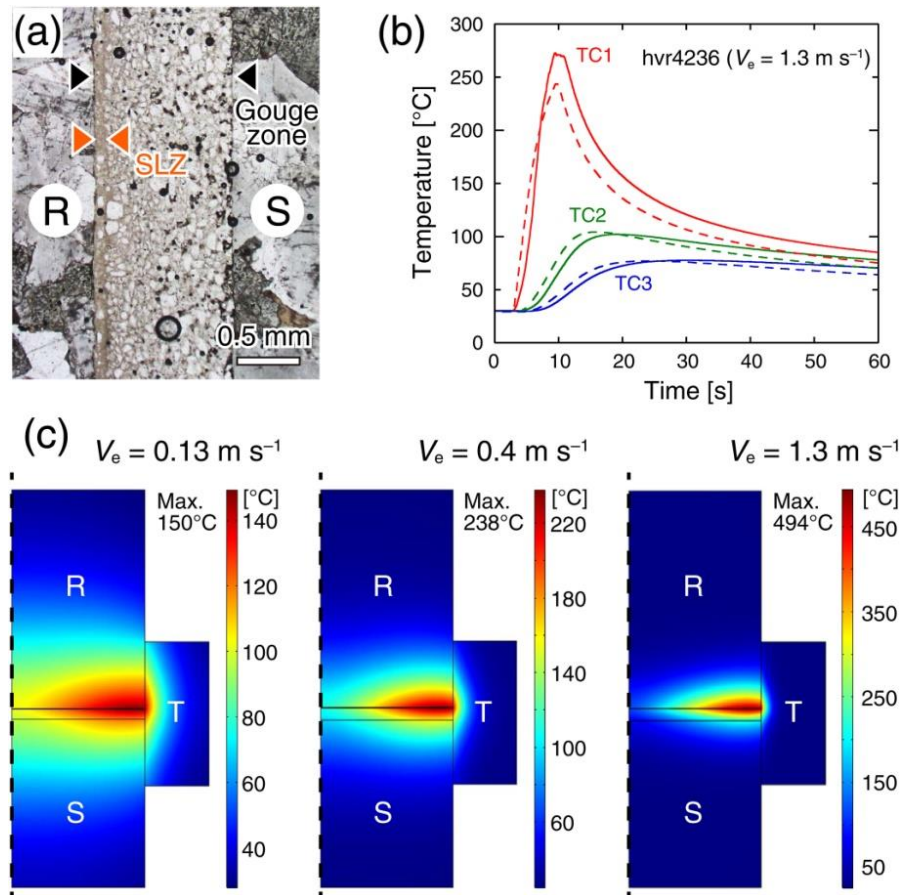
Figure 3-11. (a) Thin-section micrograph (plane-polarized light) of the gouge zone sheared at $V = 0.65$ m s^{-1}, $\sigma_n = 1.0$ MPa, $d = 10$ m, and dry conditions. A slip-localized zone (SLZ) with a thickness of ~100 μm was observed adjacent to the rotational side of the cylinder. Thin section was made perpendicular to the gouge zone about 4 mm inward from the circumference of the cylinder. (b) An example of the temporal evolution of the measured (solid line) and calculated (dashed line) temperatures where the thermocouple was placed. The depths of the thermocouples (TC1, 2, and 3) were measured to be 0.0, 3.1, and 5.0 mm using X-ray CT apparatus. (c) Representative temperature contour diagrams of specimens calculated from FEM. The left dotted line indicates the axis of rotation. R = rotational cylinder; S = stationary cylinder; T = Teflon sleeve.

Table 3-1.Summary of the Friction Experiments and the OSL Measurements Conducted in This Study

Run No.	Condition	V (m/s)	V_{sp} (m/s)	σ_n (Mpa)	d (m)	d_{sp} (m)	Δt (s)	W_F (MJ/m²)	PD (MW/m²)	Temperature [°C]			Ln/Tn (mean ± 1σ)
										TC1	TC2	TC3	
hvr4087	Dry	0.0002	0.0003	1.0	10.1	15.1	50162	6.7	0.0001	29.3	28.0	27.4	2.13 ± 1.82
hvr4092	Dry	0.0007	0.0009	1.0	10.0	13.7	15216	6.0	0.0004	28.5	27.4	26.4	2.15 ± 1.33
hvr4089	Dry	0.0013	0.0018	1.0	10.0	13.7	7620	7.3	0.0010	29.4	28.5	26.9	0.83 ± 0.66
hvr4088	Dry	0.0065	0.0091	1.0	10.1	13.4	1525	7.2	0.0047	46.7	33.8	31.3	0.62 ± 0.42
hvr4102	Dry	0.013	0.018	1.0	10.2	14.1	767	6.3	0.0086	54.1	44.4	25.4	1.72 ± 1.03
hvr4093	Dry	0.065	0.091	1.0	9.8	13.0	153	5.4	0.0351	88.6	56.7	52.5	2.27 ± 1.46
hvr4094	Dry	0.13	0.18	1.0	9.9	13.6	76.6	5.1	0.0666	118.7	76.5	58.4	2.31 ± 0.87
hvr4233	Dry	0.25	0.34	1.0	9.9	13.3	39.5	6.6	0.1681	143.3	90.8	72.3	0.35 ± 0.23
hvr4234	Dry	0.40	0.53	1.0	10.0	13.3	25.2	4.4	0.1742	155.7	90.6	66.9	0.19 ± 0.11
hvr4095	Dry	0.65	0.79	1.0	9.9	13.2	15.2	4.9	0.3206	–	–	–	0.11 ± 0.10
hvr4232	Dry	0.65	0.87	1.0	9.9	13.3	15.3	7.1	0.4683	193.4	67.7	48.6	0.11 ± 0.06
hvr4235	Dry	1.3	1.57	1.0	10.7	12.9	8.3	5.3	0.6373	181.5	91.2	55.6	0.80 ± 0.80
hvr4236	Dry	1.3	1.57	1.0	10.0	12.1	7.9	5.8	0.7352	272.7	102.0	77.6	0.01 ± 0.01
hvr4237	Water added	1.3	1.74	1.0	10.2	13.6	8.0	5.5	0.6813	192.5	108.0	84.2	0.06 ± 0.05

Note, Δt = the duration of the experoment; PD = power density.

57

Table 3-2. Single Aliquot Regenerative Dose (SAR) protocol for OSL measurement

Step	Process	Conditions	
1	Preheat	220 ℃, 10 s	–
2	OSL measurement (main measurement)	125 ℃, 60 s	Main signal (Ln)
3	X-ray irradiation	10 Gy	Test dose
4	Cut heat	180 ℃, 10 s	–
5	OSL measurement (test measurement)	125 ℃, 60 s	Test signal (Tn)

Note. Ln and Tn are derived from the initial OSL signal (1 s) minuts a background estimated from the last 1 s of the stimulation.

Table 3-3. OSL Measurement sequence

Step	
1	Hot Bleach (280 ℃ x 40 s)
2	X-ray irradiation (100, 50, 100, 0, 150, 50 Gy)
3	Preheat (180 - 260 ℃ x 10 s)
4	OSL measurement (125 ℃ x 60 s)
5	X-ray irradiation (10 Gy)
6	Cutheat (140 - 220 ℃ x 10 s)
7	OSL test measurement (125 ℃ x 60 s)
8	Return to 1

3.6 Reference

Aitken, M. J. (1985). Thermoluminescence dating. London: Academic Press.

Aretusini, S., Mittempergher, S., Plümper, O., Spagnuolo, E., Gualtieri, A. F., & Di Toro, G. (2017). Production of nanoparticles duringexperimental deformation of smectite and implications for seismic slip. Earth and Planetary Science Letters, 463, 221–231. https://doi.org/10.1016/j.epsl.2017.01.048

Banerjee, D., Singhvi, A. K., Pande, K., Gogte, V. D., & Chandra, B. P. (1999). Towards a direct dating of fault gouges using luminescencedating techniques—Methodological aspects. Current Science, 77, 256–268.

Bateman, M. D., Swift, D. A., Piotrowski, J. A., Rhodes, E. J., & Damsgaard, A. (2018). Can glacial shearing of sediment reset the signal usedfor luminescence dating? Geomorphology, 306, 90–101. https://doi.org/10.1016/j.geomorph.2018.01.017

Bulur, E. (1996). An alternative technique for optically stimulated luminescence (OSL) experiment. Radiation Measurements, 26(5),701–709. https://doi.org/10.1016/S1350-4487(97)82884-3

Di Toro, G., Han, R., Hirose, T., De Paola, N., Nielsen, S., Mizoguchi, K., et al. (2011). Fault lubrication during earthquakes. Nature,471(7339), 494–498. https://doi.org/10.1038/nature09838

Fukuchi, T. (1996). Direct ESR dating of fault gouge using clay minerals and the assessment of fault activity. Engineering Geology, 43(2–3),201–211. https://doi.org/10.1016/0013-7952(96)00061-0

Ganzawa, Y., Takahashi, C., Miura, K., and Shimizu, S. (2013). Dating of active fault gouge using optical stimulated luminescence and thermoluminescence [in Japanese with English abstract]. Journal of the Geological Society of Japan, 119(11), 714–726. https://doi.org/10.5575/geosoc.2013.0052

Guralnik, B., Ankjærgaard, C., Jain, M., Murray, A. S., Müller, A., Wälle, M., et al. (2015). OSL-thermochronometry using bedrock quartz:A note of caution. Quaternary Geochronology, 25, 37–48. https://doi.org/10.1016/j.quageo.2014.09.001

Guralnik, B., Jain, M., Herman, F., Paris, R. B., Harrison, T. M., Murray, A. S., et al. (2013). Effective closure temperature in leaky and/orsaturating thermochronometers. Earth and Planetary Science Letters, 384, 209–2218. https://doi.org/10.1016/j.epsl.2013.10.003

Hashimoto, T., Nakagawa, T. H., Hong, D.-G., & Takano, M. (2002). An automated system for both red/blue thermoluminescence andoptically stimulated luminescence measurement. Journal of Nuclear Science and Technology, 39(1), 108–109. https://doi.org/10.1080/18811248.2002.9715163

Hiraga, S., Morimoto, A., & Shimamoto, T. (2002). Stress effect on thermoluminescence intensities of quartz grains—For the establishmentof a fault dating method—. Bulletin of Nara University of Education Natural Science, 51(2), 17–24.

Hiraga, S., Yoshimoto, A., & Shimamoto, T. (2004). TL intensity changes of fine-grained quartz gouge

during frictional sliding: Completezeroing depth estimated from the result of shear experiments. Nara University of Education, 53(2), 17–29.

Hirose, T., & Shimamoto, T. (2005). Growth of molten zone as a mechanism of slip weakening of simulated faults in gabbro during frictionalmelting. Journal of Geophysical Research, 110, B05202. https://doi.org/10.1029/2004JB003207

Ide, S., & Takeo, M. (1997). Determination of constitutive relations of fault slip based on seismic wave analysis. Journal of GeophysicalResearch, 102(B12), 27,379–27,391. https://doi.org/10.1029/97JB02675

Ikeya, M., Miki, T., & Tanaka, K. (1982). Dating of a fault by electron spin resonance on intrafault materials. Science, 215(4538), 1392–1393.https://doi.org/10.1126/science.215.4538.1392

Jain, M., Murray, A. S., & Bøtter-Jensen, L. (2003). Characterisation of blue-light stimulated luminescence components in differentquartz samples: Implications for dose measurement. Radiation Measurements, 37(4–5), 441–449. https://doi.org/10.1016/S1350-4487(03)00052-0

Jeong, G. Y., & Choi, J.-H. (2012). Variations in quartz OSL components with lithology, weathering and transportation. QuaternaryGeochronology, 10, 320–326. https://doi.org/10.1016/j.quageo.2012.02.023

Kim, J. H., Ree, J.-H., Choi, J.-H., Chauhan, N., Hirose, T., & Kitamura, M. (2019). Experimental investigations on dating the last earthquakeevent using OSL signals of quartz from fault gouges. Tectonophysics, 769, 228191. https://doi.org/10.1016/j.tecto.2019.228191

Kitajima, H., Chester, J. S., Chester, F. M., & Shimamoto, T. (2010). High-speed friction of disaggregated ultracataclasite in rotary shear:Characterization of frictional heating, mechanical behavior, and microstructure evolution. Journal of Geophysical Research, 115, B08408.https://doi.org/10.1029/2009JB007038

Kralik, M., Klima, K., & Riedmüller, G. (1987). Dating fault gouges. Nature, 327(6120), 315–317. https://doi.org/10.1038/327315a0

Mizoguchi, K., Hirose, T., Shimamoto, T., & Fukuyama, E. (2009). High-velocity frictional behavior and microstructure evolution of faultgouge obtained from Nojima fault, southwest Japan. Tectonophysics, 471(3–4), 285–296. https://doi.org/10.1016/j.tecto.2009.02.033

Murakami, M., & Tagami, T. (2004). Dating pseudotachylyte of the Nojima fault using the zircon fission-track method. GeophysicalResearch Letters, 31, L12604. https://doi.org/10.1029/2004GL020211

Murray, A. S., & Wintle, A. G. (1999). Isothermal decay of optically stimulated luminescence in quartz. Radiation Measurements, 30(1),119–125. https://doi.org/10.1016/S1350-4487(98)00097-3

Murray, A. S., & Wintle, A. G. (2000). Dating quartz using an improved single-aliquot regenerative-dose (SAR) protocol. Radiation Measurements, 32(1), 57–73. https://doi.org/10.1016/S1350-4487(99)00253-X

Nishiwaki, T., & Lin, A. (2019). Fractures and subsidiary faults developed in the active strike-slip Nojima fault zone, Japan, and tectonicimplications. Tectonics, 38, 4290–4300. https://doi.org/10.1029/2018TC005391

Oohashi, K., Hirose, T., & Shimamoto, T. (2013). Graphite as a lubricating agent in fault zones: An insight from low- to high-velocityfriction experiments on a mixed graphite-quartz gouge. Journal of Geophysical Research: Solid Earth, 118, 2067–2084. https://doi.org/10.1002/jgrb.50175

Oohashi, K., Minomo, Y., Akasegawa, K., Hasebe, N., & Miura, K. (2019). OSL signal zeroing of quartz gouge during sub-seismic to seismicfrictional sliding—Data. Open Science Framework. https://doi.org/10.17605/OSF.IO/35REB

Shimamoto, T., & Tsutsumi, A. (1994). A new rotary-shear high-velocity friction testing machine: Its basic design and scope of research [inJapanese with English abstract]. Jour. Tectonic Res. Group Japan, 39, 65–78.

Singarayer, J. S., & Bailey, R. M. (2003). Further investigations of the quartz optically stimulated luminescence components using linearmodulation. Radiation Measurements, 37(4–5), 451–458. https://doi.org/10.1016/S1350-4487(03)00062-3

Smedley, R. K. (2018). Telling the time with dust, sand and rocks. Elements, 14(1), 9–14. https://doi.org/10.2138/gselements.14.1.9

Togo, T., & Shimamoto, T. (2012). Energy partition for grain crushing in quartz gouge during subseismic to seismic fault motion: Anexperimental study. Journal of Structural Geology, 38, 139–155. https://doi.org/10.1016/j.jsg.2011.12.014

Tsukamoto, S., Tagami, T., & Zwingmann, H. (2020). Direct dating of fault movement. In D. Tanner, & C. Brandes (Eds.), Understandingfaults—Detecting, dating, and modeling (pp. 257–278). Amsterdam: Elsevier. https://doi.org/10.1016/B978-0-12-815985-9.00007-2

Vermeesch, P. (2012). On the visualisation of detrital age distributions. Chemical Geology, 312–313, 190–194. https://doi.org/10.1016/j.chemgeo.2012.04.021

Wintle, A. G., & Murray, A. S. (2006). A review of quartz optically stimulated luminescence characteristics and their relevance in singlealiquotregeneration dating protocols. Radiation Measurements, 41(4), 369–391. https://doi.org/10.1016/j.radmeas.2005.11.001

Wölfler, A., Kurz, W., Danišík, M., & Rabitsch, R. (2010). Dating of fault zone activity by apatite fission track and apatite (U–Th)/Hethermochronometry: A case study from the Lavanttal fault system (Eastern Alps). Terra Nova, 22, 274, no–282. https://doi.org/10.1111/j.1365-3121.2010.00943.x

Yamada, R., Matsuda, T., & Omura, K. (2007). Apatite and zircon fission-track dating from the Hirabayashi-NIED borehole, Nojima Fault, Japan: Evidence for anomalous heating in fracture zones. Tectonophysics, 443(3–4), 153–160. https://doi.org/10.1016/j.tecto.2007.01.014

Yang, H. L., Chen, J., Yao, L., Liu, C. R., Shimamoto, T., Ann, J., & Thompson, J. A. (2019). Resetting

of OSL/TL/ESR signals by frictionalheating in experimentally sheared quartz gouge at seismic slip rates. Quaternary Geochronology, 49, 52–56. https://doi.org/10.1016/j.quageo.2018.05.005

Yao, L., Shimamoto, T., Ma, S., Han, R., & Mizoguchi, K. (2013). Rapid post seismic strength recovery of Pingxi fault gouge from the Longmenshan fault system: Experiments and implications for the mechanisms of high-velocity weakening of faults. Journal of Geophysical Research: Solid Earth, 118, 4547–4563. https://doi.org/10.1002/jgrb.50308

Zwingmann, H., & Mancktelow, N. (2004). Timing of Alpine fault gouges. Earth and Planetary Science Letters, 223, 415–425. https://doi.org/10.1016/j.epsl.2004.04.041

CHAPTER 4

4.Luminescence measurements using deep borehole cores from the Nojima Fault and the Asano Fault (a companion fault to the Nojima Fault)

4.1 Introduction

As are shown in chapter 2 and 3, the surface fault gouge is not suitable to detect the latest activity of the fault. Therefore, this chapter discusses the importance of deep borehole investigations.

In Chapter 2, luminescence signals were investigated using samples extracted from the surface of the fault plane. As already mentioned, the results did not give a date of 1995 (approximately 30 years ago), that is the last active period of the fault, even for samples extracted from the fault gouge. This may be because the fault gouge quartz samples taken from the surface have not reached the conditions necessary to completely reset the accumulated luminescence signal (zero reset). Chapter 3 suggested the conditions necessary for zero-resetting by frictional energy associated with faulting activity. Ganzawa et al. (2013) also suggested certain temperature conditions necessary for zero-reset of luminescence signal. Therefore, it is possible that the luminescence signal accumulated in quartz is zero-reset if the fault plane was active at a deeper level where the ambient temperature is high.

In this chapter, core samples obtained during deep borehole investigations on the Asano and Nojima Faults were used. The objective of this chapter is to assess the degree of resetting of accumulated dose of quartz samples at the presumed fault plane in the cores using the TL and OSL methods.

4.2 Drilling site and measurement samples

The drilling locations of the deep boreholes are shown in Figure 4-1. The borehole cores drilled on the Asano Fault were called AFD and anlysed samples were AFD-1 to 4. The borehole cores drilled on the Nojima Fault were called NFD-1 and 2, and the additional NFD cores were called as S1 to S4.For deep fault core measurements, AFD2-8 (8.5 m) and AFD2-103 (1.3 m) are non-destructive granites from the AFD2 core from the Asano fault drilling core. The samples fa-1-118.58 (118.58 m), fa-1-118.60 (118.60 m) and fa-1-white (gouge 118.59 m) (Figure. 4-2) andAFD2 fa-5 (203.16 m) (Figure. 4-3) were analysed in the study. Drilled cores from the Nojima Fault show several fault planes, and NFD1 S4 [604.85-605.65 m, Figure 4-4], NFD1 S2 [727.5-727.7 m, Figure 4-5], NFD2 [321.0-321.6 m, Figure 4-6]) and deeper samples which is considered unaffected by fault activity (NFD1 966 [966 m] (Figure 4.7) and NFD1 S3 800 [800 m](Figure 4-8), as well as the Tsushigawa Granite (TS), which is the base rock of the study area are analysed. Please mind that numerical values in brackets are core length, not depth. The core samples used in this chapter were kept in a dark room near the drilling site after drilling, where the samples were to be sketched and processed into samples for other studies. Therefore, the effect on the light source luminescence signal used in the darkroom is also

being investigated.

4.3 Luminescence measurement
4.3.1 Equipment and methods

The equipment and TL measurement protcol is described in Chapter 2. In addition, blue TL (BTL) measurement was carried out with BG-39 (schoot) filter. The OSL measurement conditions and protocol were described in Chapter 3. The details of newly introduced measurements in this chapter are described in this section.

4.3.2 Evaluation of light sources in dark room

The cores are stored in wooden boxes that are specially designed to block external light, so the likelihood of light exposure during storage is very low. The investigation of the core lithology, however, was carried out in a dark room under a reddish light over a long period of time. Therefore, an investigation was carried out to determine whether long-term light exposure causes attenuation of the luminescence signal. The samples used were granite sludge obtained during drilling and standard quartz sample for luminescence dating.

In the light-exposure experiments the samples were exposed to three different light sources in addition to the non-light-exposed samples. The samples were Block (non-light-exposed samples), Photo (exposed to a photographic device), LED (exposed to an LED flashlight) and Toshiba (exposed to a Toshiba red light source). For the camera flash and LED flashlight exposures, the distance to the light source and exposure time were set to simulate photography. For the LED light source, the exposure time was set to 2 min from a point about 1.2 m away. In the exposure experiment using a Toshiba red light source, the exposure time was set to approximately 20 minutes, considering the actual working time under the red light source. The samples were subjected to mineral separation in the dark room and quartz was extracted. OSL and TL analyses were carried out by picking up 15 quartz particles of 250 μm or less in size.

Luminescence was also measured after exposure to artificial radiation of approximately 5 Gy to determine the luminescence properties of the samples. The pre-heat condition for this measurement was 180°C for 10 seconds. Three discs of each sample were measured. The BTL measurements were carried out at temperatures between 100°C and 450°C. The samples were also irradiated with 100 Gy of X-rays in order to observe changes in luminescence properties. As in the usual quantitative analysis of accumulated doses, measurements were also carried out by irradiating the samples with 100 Gy, 200 Gy, 300 Gy and 100 Gy of X-rays, and changes in signal shape were observed.

To more rigorously assess only the effects of light exposure, luminescence standard quartz provided by Riso, whose luminescence properties are well known, was used: samples exposed to approximately 10 Gy of X-rays were prepared for the OSL measurement and 100 Gy for the TL

measurement, respectively. Light exposure experiments on the samples were carried out in a dark room at the core drilling site.

For the standard quartz samples for luminescence, the degree of attenuation was also evaluated by performing actual dose measurements using the OSL method. The average equivalent dose measurement for the samples used is 4.70 ± 0.14 Gy. The light exposure conditions were the same with explanation above. For equivalent dose measurements, the SAR method was used. The pre-heating at 220 °C for 10 s and the cut-heating at 180 °C for 10 s with a test irradiation of 5 Gy were applied. Artificial irradiations for calibration curves were 2.7 Gy, 0 Gy, 5 Gy, 10 Gy and 5 Gy. Three discs of were measured for each sample and the average equivalent dose was calculated. In total, more than 170 OSL measurements and about 60 TL measurements were performed.

4.3.3 Luminescence measurements of core samples

Accumulated doses of quartz were calculated for the samples listed in 4-2; all TL and OSL measurements were made using the SAR method (Wintle and Murray., 2006) (Table 3-5). In addition, LM-OSL measurements were also performed for some of the samples for which OSL measurements were made, and the emission components were analysed.

4.4 Result and discussion

4.4.1 Darkroom evaluation of light sources in use

Photo-exposure experiments were carried out on standard quartz samples irradiated with approximately 10 Gy of X-rays (for OSL measurements) and approximately 100 Gy of X-rays (for TL measurements). Typical results are shown in Figures 4-9. and Figure 4-10.

The results of the OSL measurements (Figure 4-9.) show that all samples still suffered signal decrease due to exposure, but the fast component was only attenuated by about 15% by the photographic and LED light sources, partly because the exposure time was short. On the other hand, the Toshiba red light source cause the loss of the fast component by less than half, probably due to a long exposure time during the observation.

The results of the TL measurements (Figure 4-10.) show that the luminescence emission characteristics of the non-light-exposed samples of each sample are different. The luminescence temperature is common for all samples, with peaks at approximately 200 °C and 320 °C, but the peak ratios are slightly different and the signal is attenuated for all samples. The least affected is the exposure to the camera flash, which shows no attenuation of the signal at high temperatures, but only at low temperatures.

Finally, Table 4-1. shows the results of the evaluation of the degree of attenuation by performing actual dosimetry using the OSL method on the standard quartz samples for luminescence as described above. The results show that the attenuation due to Toshiba exposure is clear and that the influence of

the attenuation due to the light source of the camera is the smallest.

Figure 4-11. (a) shows that the natural sample does not retain the OSL signal. The absence of signal in the non-light-exposed samples (Block) also suggests that these samples either do not retain the luminescence signal or that the signal has been lost due to drilling. The results of OSL measurements on these samples after exposure to approximately 5 Gy of X-rays are shown in Figure 4-11. (b). The results show differences in the intensity of the emission. The results show that the sample itself is capable of OSL emission, although there are differences in the intensity of the emission.

Next, comparing the results of the TL measurements of the natural sample (Figure 4-12. (a)) with the results of the BTL measurements (Figure 4-12. (b)) after exposure to approximately 100 Gy of X-rays, no signals at temperatures lower than about 200°C were detected in the natural sample. It is likely that the sludge samples were directly subjected to friction during drilling, and therefore the signal was lost during sample collection.

Further OSL analysis was carried out on samples that had not undergone drilling (BR), granite quartz samples collected in outcrop and core samples that were not sludge (Test core)(Figure 4-13.). Natural signals were observed in all samples. Therefore, the significantly smaller natural signal in the sludge samples could be attributed to the bit blade being hit during drilling.

4.4.2 Luminescence measurements of core samples
4.4.2.1 Asano fault core

A representative result of the T-Tmax method performed on AFD2 fa-1 and a UV-TL emission curve are shown in Figure 4-14. No clear TL site temperature could be calculated for any of the samples used in this study. This result is similar with the trench sample close to the fault gouge (S7). Therefore, the emission curves obtained using the site temperatures used in Chapter 2 (200°C, 270°C, 340°C and 400°C) were peak-separated and the signals corresponding to each temperature were used to create a calibration curve to determine the accumulated dose.

In AFD2 fa-1, the main gouge and its upper and lower parts were analysed separately, and six replicates of each of the three aliquoted samples were measured, but some of the samples did not generate a calibration curve properly. Those data were excluded from the calculation of averages (Table 4-2), and no particular differences were found between the three samples. The accumulated doses in the mid-temperature range from 270°C to 360°C were comparable to those obtained from the analysis of the original rock described above, and no resetting of the age values could be detected. Therefore, the TL signal of this analysed gouge does not appear to have been affected by the 1995 earthquake.

The accumulated dose was estimated for AFD2 fa-5 5 (Table 4-2), but it was difficult to separate quartz and only one aliquot was measured for each sample. AFD2 fa-5 5-3 is the main gouge, but the TL signal still did not show any reduction in accumulated dose. The accumulated dose by the OSL

method was lower than that by the TL method and showed the same tendency as that of the AFD2fa-1 sample. The accumulated dose by the OSL method was lowest in the main gouge sample (AFD2 fa-5 5-3), which may be due to faulting.

Accumulated doses obtained from the TL method in the mid-temperature range in the trench samples show lower values near the fault, which may be due to some fault effects, although it is not clear if this is due to the 1995 earthquake or not.

It is also possible that both of these two fracture zone samples were either inactive during the 1995 earthquake, or that they were active but did not suffer enough energy to reset the accumulated dose to zero at this depth condition.

4.4.2.2 Nojima fault core

The Nojima Fault core samples were measured only by OSL based on the results of the previous chapter and the amount of samples collected was very small. First, the results of three samples that are considered to be almost unaffected by fault activity are presented.

NFD1 966, NFD1 S3 800, and Tsushigawa Granite (TS)

Examples of OSL and LM-OSL measurements for each are shown in Figure 4-15 to Figure 4-17. The granite has quartz with predominant ultrafast components, while some TS and NFD1 S3 800 had no ultrafast components (Figure 4-15. and Figure 4-16.), while the deepest sample, NFD1 966, had ultrafast components in all measured samples (Figure 4-17.) The TS and NFD1-S3 800, the accumulated doses varied between samples with and without an ultrafast component, with samples with an ultrafast component having slightly higher accumulated doses (Table 4-3.). The variation in accumulated dose is similar to the results in Chapter 2. The accumulated dose tends to be smaller in samples from deeper sites, but the variation in accumulated dose in all samples makes it difficult to determine the effect of geothermal heat at different depths.

Gouge core samples

The results are described in the order of shallow to deep samples.

Although LM-OSL measurements could not be performed on NFD2 samples, no ultrafast component was expected from the shape of the emission. The accumulated dose for this sample ranged from about 1-10 Gy (Table 4-4.). The samples (1 and 2A) considered to be the main fault axis (boundary between 1 and 2) have values of about 5-10 Gy, which do not coincide with the area showing the lowest accumulated doses, and these values are comparable to those expected for healthy rocks at the same depth (without ultrafast component of the TS). Adjacent samples (2B and 3) show lower values of 0.8 to 2 Gy. These values are predominantly lower than the expected values for healthy rock at the same depth.

Next, NFD1 S4 had no ultrafast component as a result of LM-OSL measurements (Figure 4-18.). Compared to the results for the Base Rock sample described above, which showed an accumulated dose of approximately 20-70 Gy (Table 4-5), no decrease in accumulated dose could be observed. Nor does the result show that only the fault main axes show lower values.

NFD1 S2 had LM-OSL measurements with and without an ultrafast component (Figure 4-19.). This sample showed the lowest accumulated dose of approximately 0.2-1.5 Gy (Table 4-6.). This result is lower than that of the healthy rock (NFD1-S3), which was obtained from a deeper depth than this sample. This may be a result of the sample being affected by faulting activity. The accumulated doses in the surrounding samples (1 and 3) are lower than in the gouge sample (2).

The annual doses estimated from the K, U, Th and Sr concentrations are shown in Table 4-7. The annual doses varied between samples with large variation in concentrations of uranium and thorium, with values ranging from 5.4-15.0 Gy/kyr and an average value of 8.5 Gy/kyr (Table 4-8). Age estimates using each accumulated dose and the average annual dose indicate that the fault is less than 50 years old and was active during the Southern Hyogo earthquake.

The deepest sample, NFD1 966 (2-5), including the gouge, had almost no ultrafast component, unlike the nearby Base Rock (Fig. 4-7.). Values were lowest just above the gouge and slightly lower than those of the Base Rock (Table 4-9.). Values just below the gouge were also considerably larger than those of the Base Rock. These values may be characteristic of the cataclasite, as they are similar to the two values found in the trench samples. The cause for the higher values than the Base Rock is not clear, but there is a possibility of deformation increases the apparent dose.

The fact that there was no decrease in the accumulated dose in the gouge taken from the main fault axis of the NFD1-S2 sample, which had the lowest accumulated dose, and NFD-2 and NFD1-S4, which are presumed to be the main Nojima fault, suggests that the gouge had already developed before the most recent earthquake and was easily deformed (flowed) in response to stress by the latest earthquake. This let the energy by fault activity was leaked by deforming (flowing), and the luminescence signal was not reset to zero.

As mentioned above, developed parts of the gouge probably do not generate a signal reset due to frictional heat because the energy is dispersed by the deformation (flow) of the gouge. For age determination, it is preferable to analyse samples from faults with less developed gouge, and in the immediate vicinity of the gouge rather than the gouge itself. On the other hand, by analogy with the results from the trenches and the deepest samples of the Nojima core, the apparent dose may increase if only rupture occurs without a temperature increase by frictional heat.

The OSL signal decreases at deeper depths due to the influence of higher ambient temperature. Therefore, when assessing the timing of the last activity of a fault, it is important to carry out a comparison with healthy rock at a considerable distance from the fault to assess whether the effect is due to the fault or due to the ambient temperature at depths. Although the signal is more likely to reset

completely at higher geothermal temperatures, the lowest accumulated dose of 0.78 Gy in sample NFD-2 at a depth of about 300 m analysed in this study is dated as about 90 years ago. Therefore, at this depth, the signal is considerably reduced, although it was not a complete reset. On the other hand, sample NFD-1-S2, at a depth of approximately 700 m, gave a value that was probably a near-complete reset. It is difficult to say at which depth the samples should be collected due to the influence of the geothermal temperature in the study area and the degree of thermal influence by faults, but in the case of the Nojima area, the boundary is thought to be between 300 m and 700 m.

4.5 Summary

For historically unknown active faults, errors of around 100 years are acceptable, so samples from a depth of around 300 m may be sufficient for evaluation. However, this is not the case for older faults, where a uplifting of more than 300 m is expected. A reset age could not be detected even in the sample from the Asano fault (200 m depth), but this could be because the depth of the sample was not sufficient, there may have been a problem with the identification of the fault. In the future, it will be necessary to evaluate the geothermal effects (collection of information shallower than 800 m), to verify the hypothesis at the Nojima fault by analysing samples close to the gouge at the Asano fault, and to evaluate the degree of resetting of the age values at each depth.
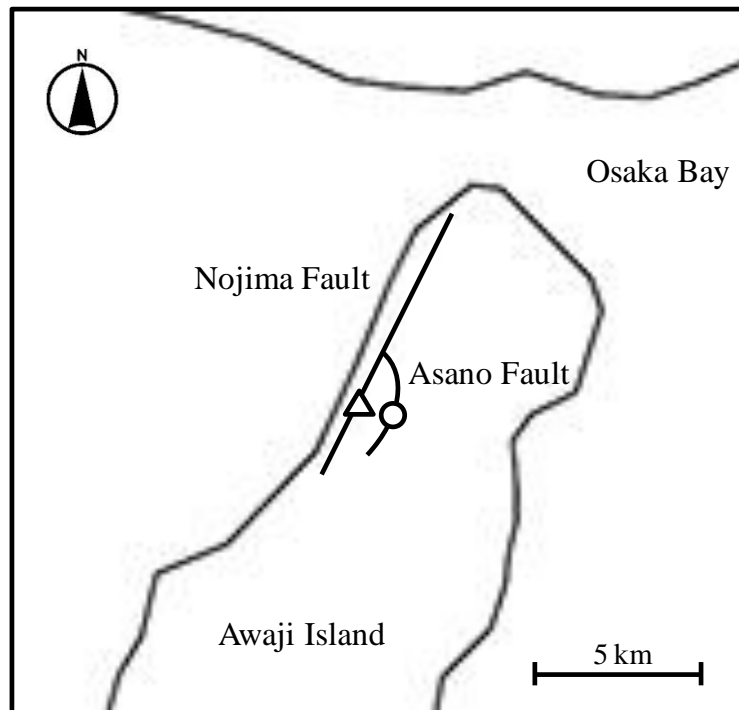
Figure 4-1. Borehole Samples localities (outline drawing).
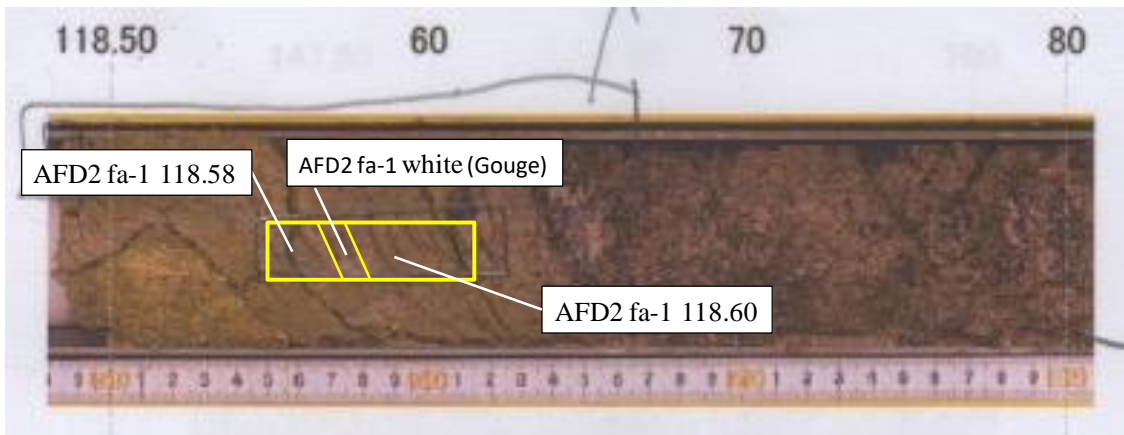
Circular AFD, triangular NFD
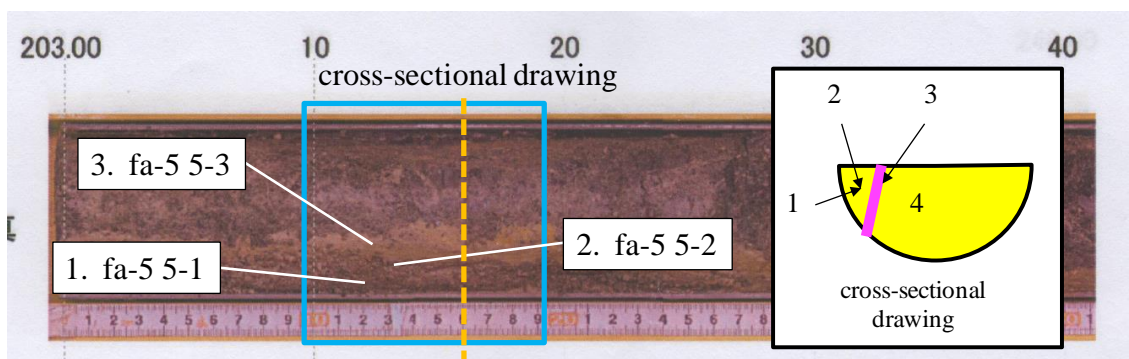
Figure 4-2. AFD2 fa-1 core

Figure 4-3. AFD fa-5 core. 5-1.0.5 cm from outer circumference, 5-2.Gouge proximity division, 5-3.Gouge, 5-4.Rock body away from the gouge
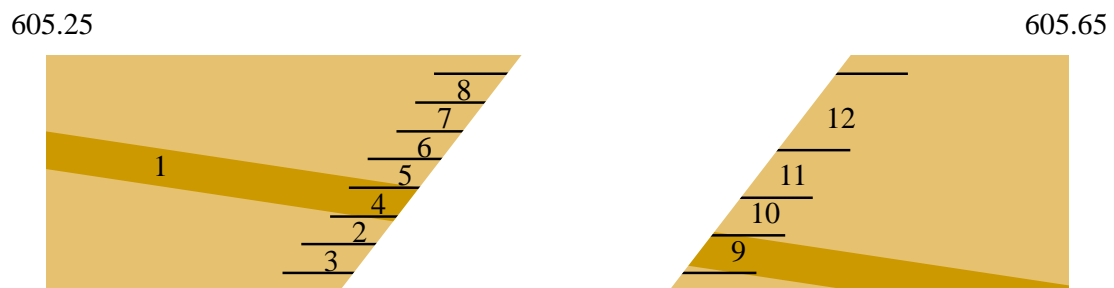
Figure 4-4. NFD2 core (outline drawing). Dark-coloured areas are considered to be gouge areas.

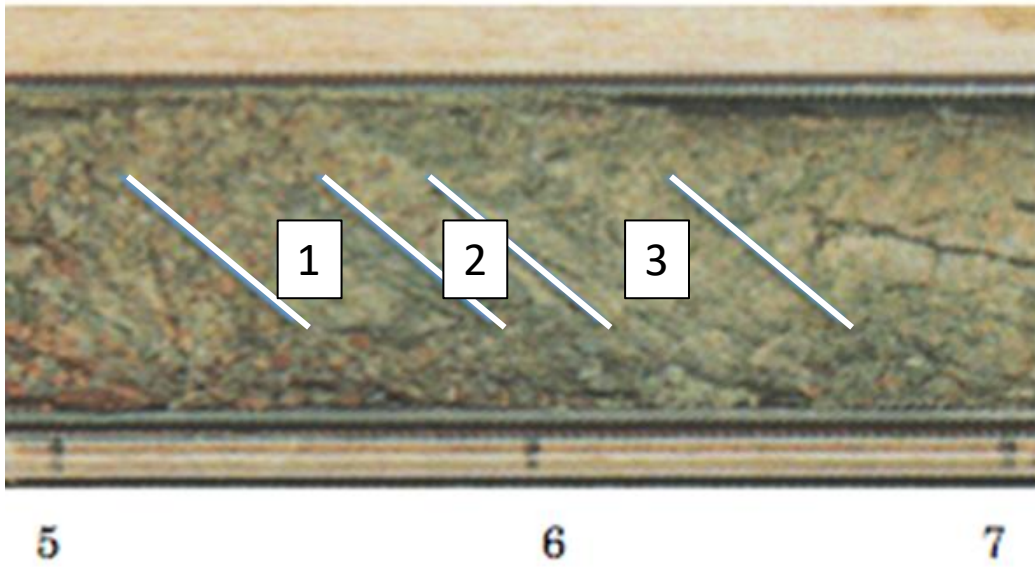Figure 4-5. NFD1 S2 core. The line between 1 and 2 is considered to be the gouge.

Figure 4-6. NDF2 core. The gouge is considered to be position 2. The 2 position is divided into equal parts, with the 1 position side being position 2A and the 3 position side being position 2B.

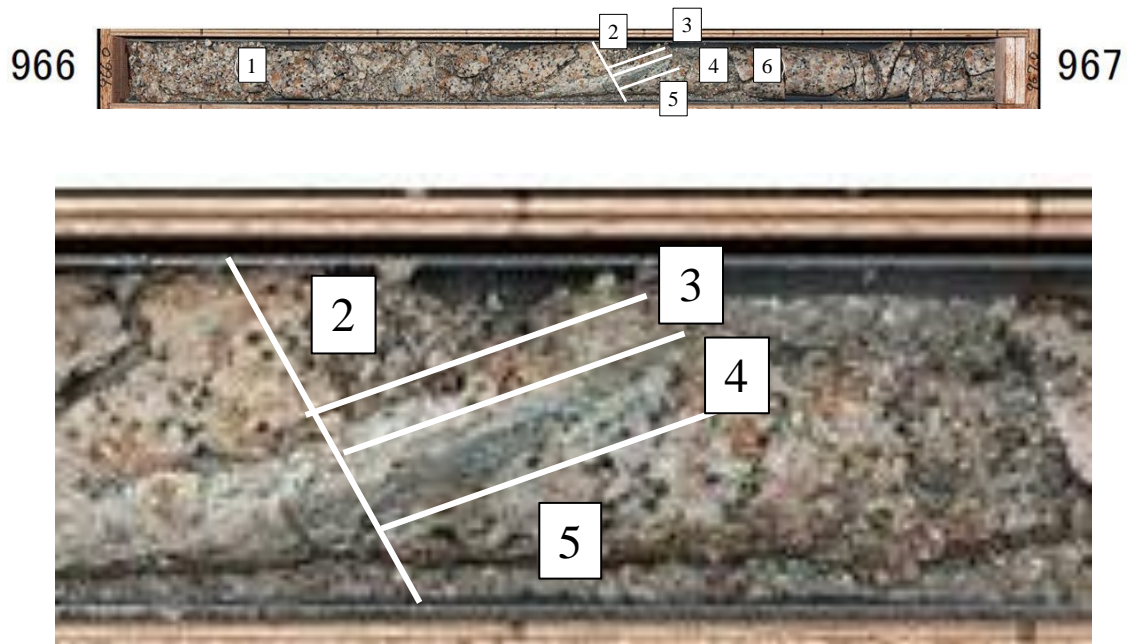Figure 4-7. Samples taken from the part of NFD1 966 containing the gouge. Bottom: close-up view of the sample. 1: area away from the gouge, 2: area containing the gouge 3: area just above the gouge 4: area just below the gouge 5: area just below the gouge 6: area sampled by other research groups.

Figure 4-8. NFD1 800 core. The outer periphery was removed and only the centre was used for luminescence measurements.

Figure 4-9. Results of light exposure experiments on samples equivalent to 10 Gy (OSL).

From top to bottom: photo light exposure, LED light exposure, and Toshiba red light. Red
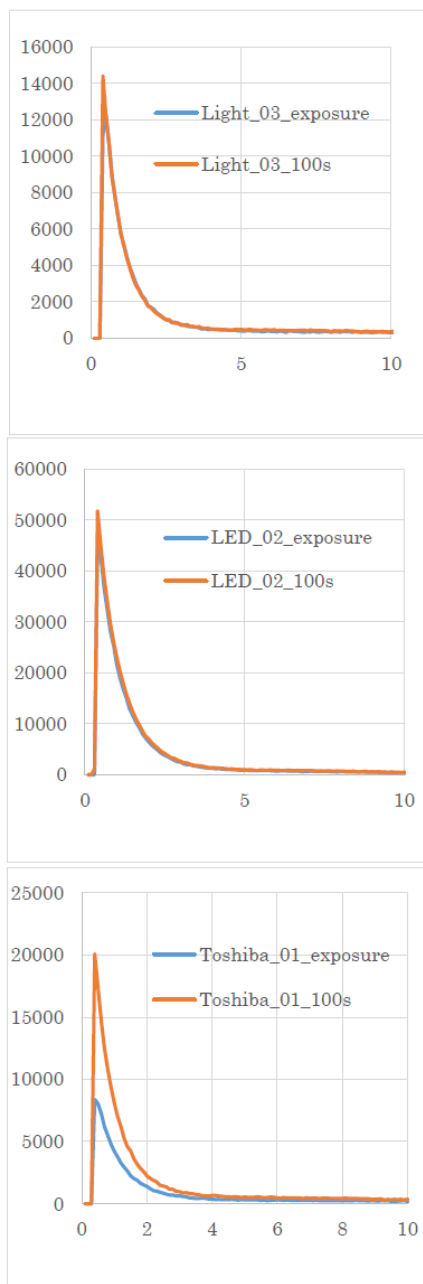
is the signal for non-photo-exposure and blue for photo-exposure.
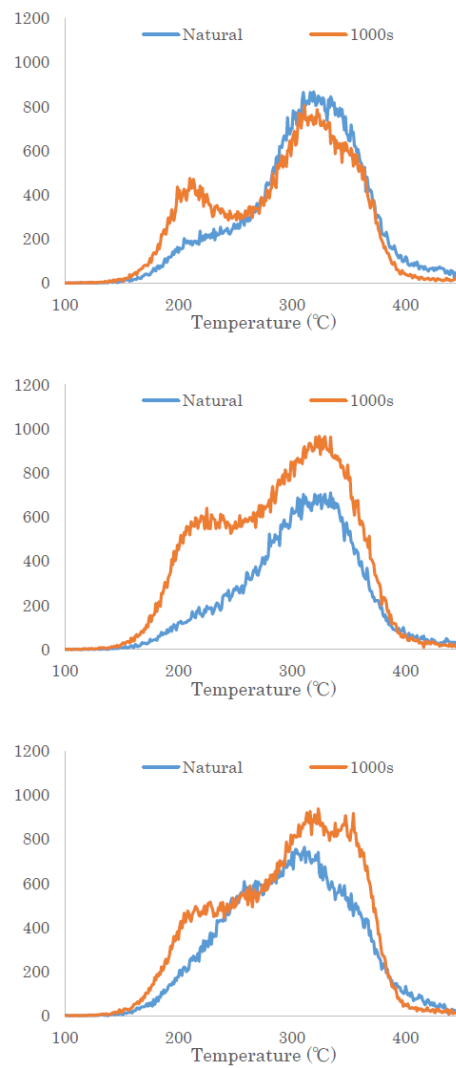
Figure 4-10. Results of light exposure experiments on samples equivalent to 100 Gy (TL). From top: photo light exposure, LED light exposure,. Toshiba red light. Red is the signal for non-photo-exposure and blue for photo-exposure.
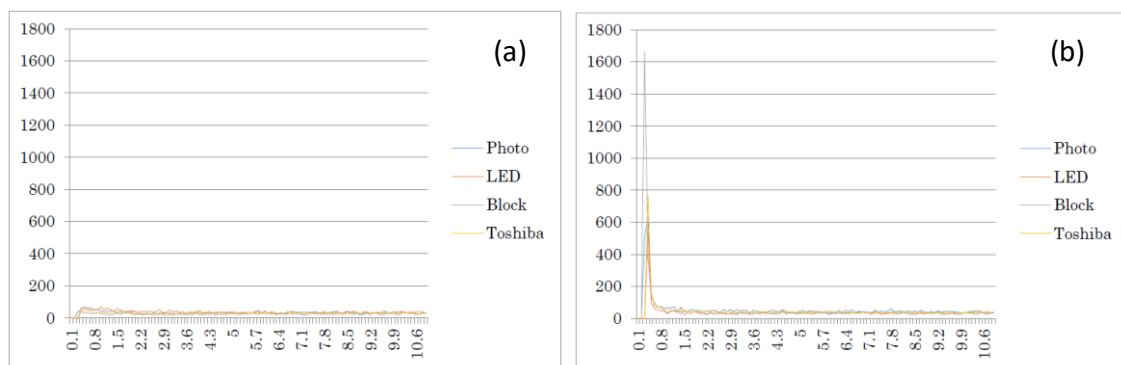
Figure 4-11. OSL measurement results . a; Natural OSL content of light-exposed samples. Vertical axis: signal intensity, b; OSL content when exposed to 5 Gy of X-rays.
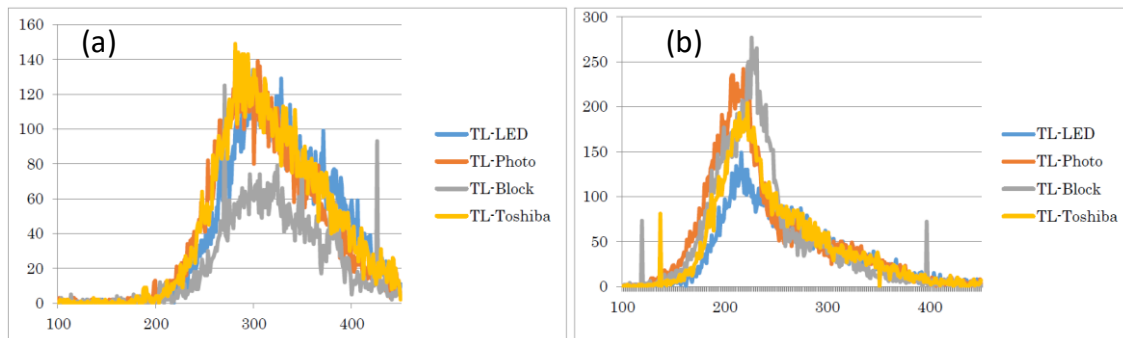
Figure 4-12. TL measurement results . a; Natural OSL content of light-exposed samples. Vertical axis: signal intensity, b; OSL content when exposed to 100 Gy of X-rays.
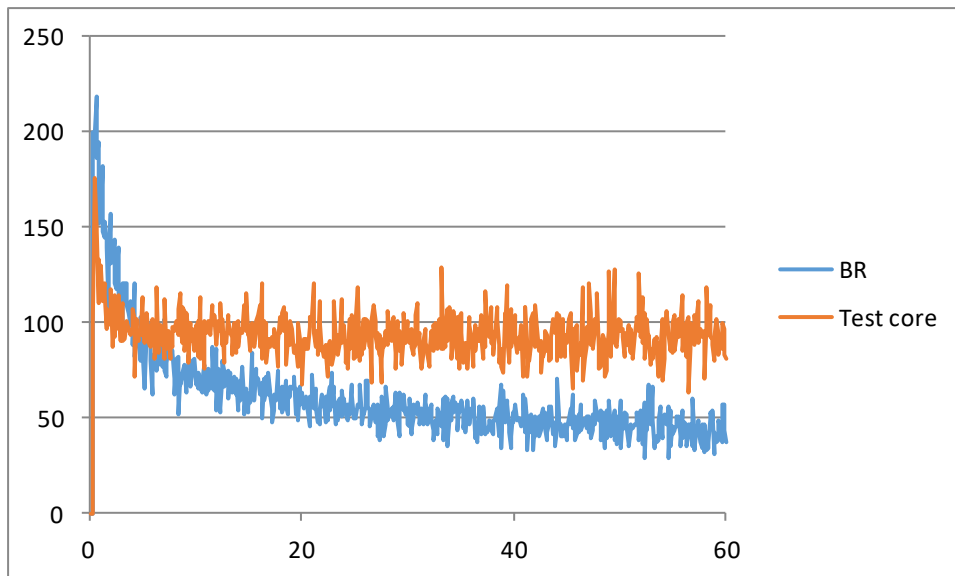
Figure 4-13. OSL measurement results . BR (base rock) and Test core (test sample taken from borehole).
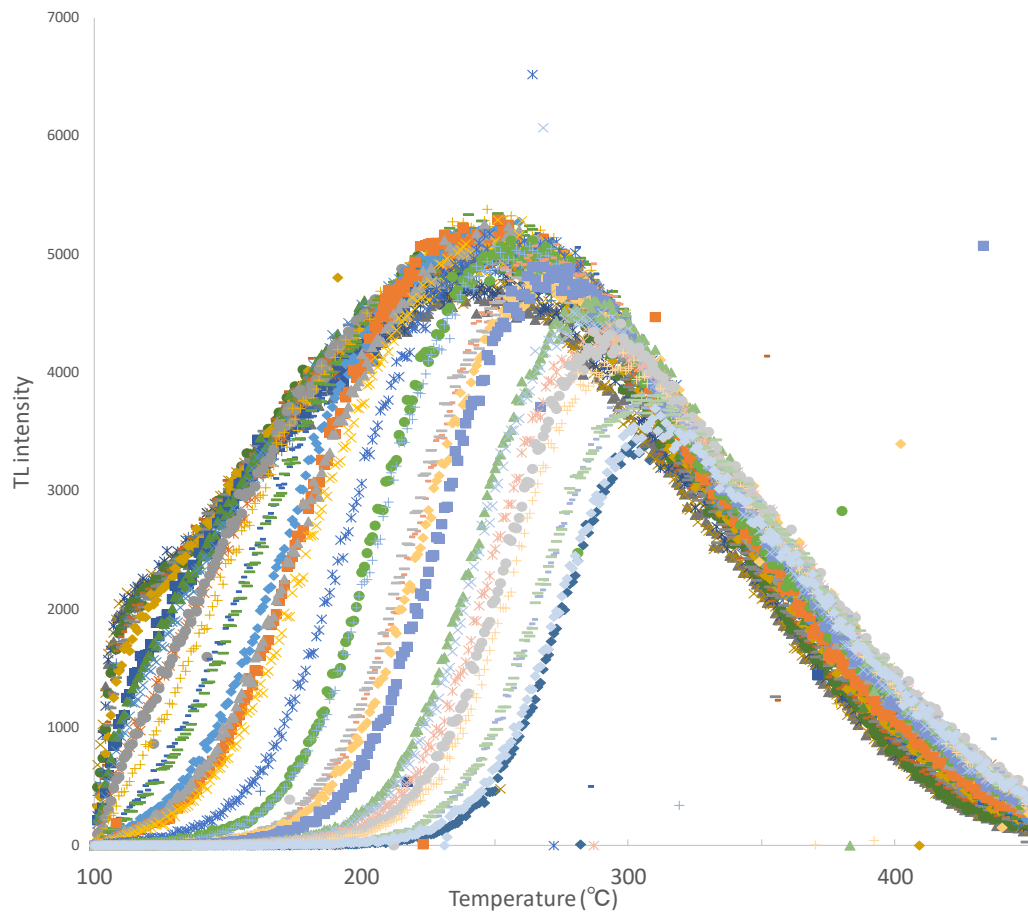
Figure 4-14. Example TL emission curves of AFD2 fa-1 samples measured using the T-Tmax method.
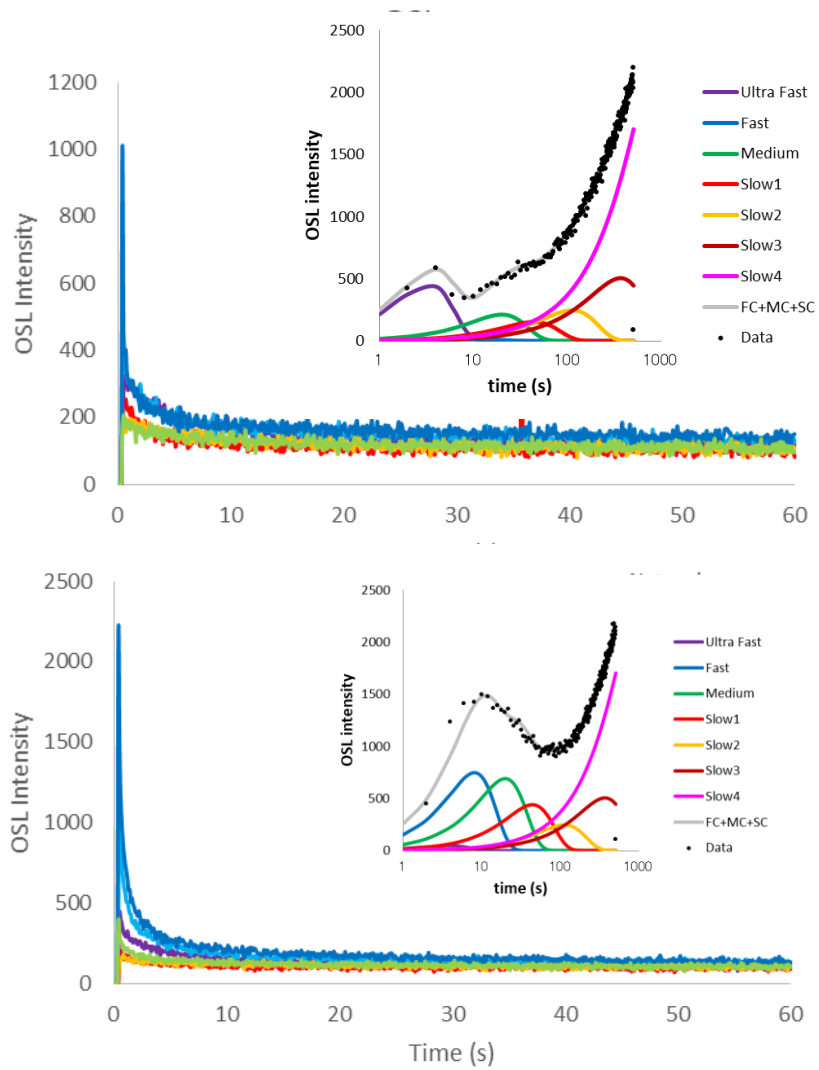
Figure 4-15. Examples of OSL and LM-OSL measurements on the Tushigawa granite (TS).Top data shows an ULTRA FAST component.
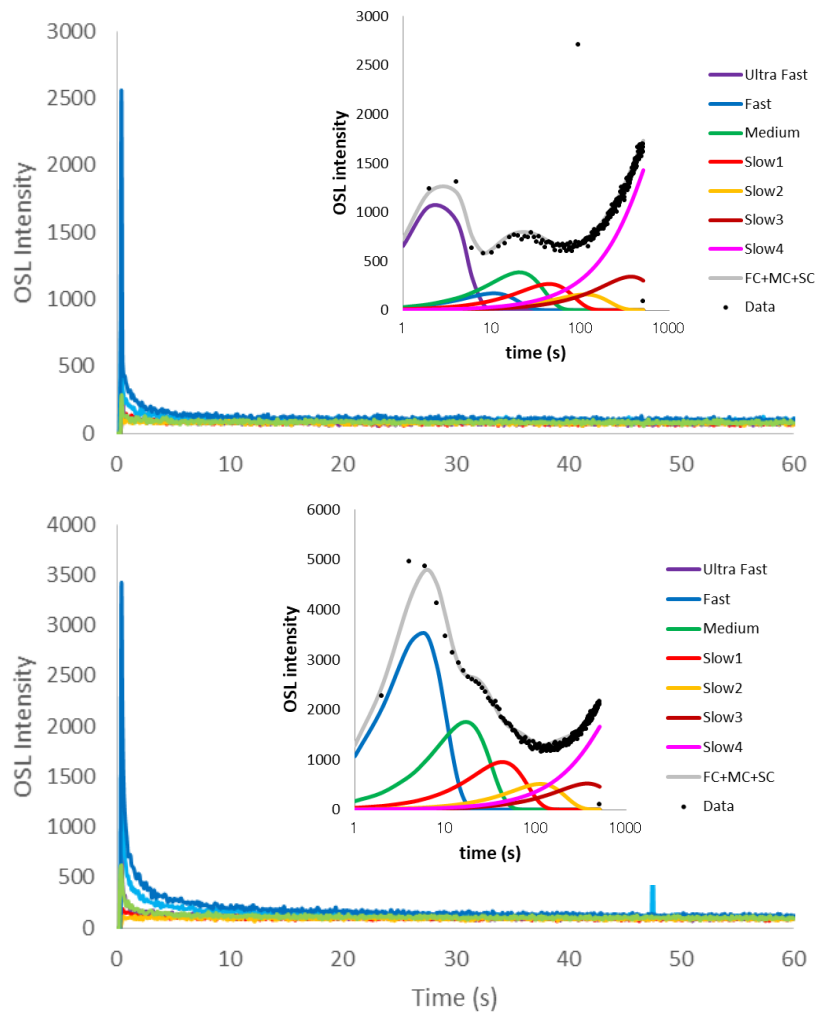
Figure 4-16. Examples of NFD1 S3 800 OSL and LM-OSL measurements. Top data shows an ULTRA FAST component.
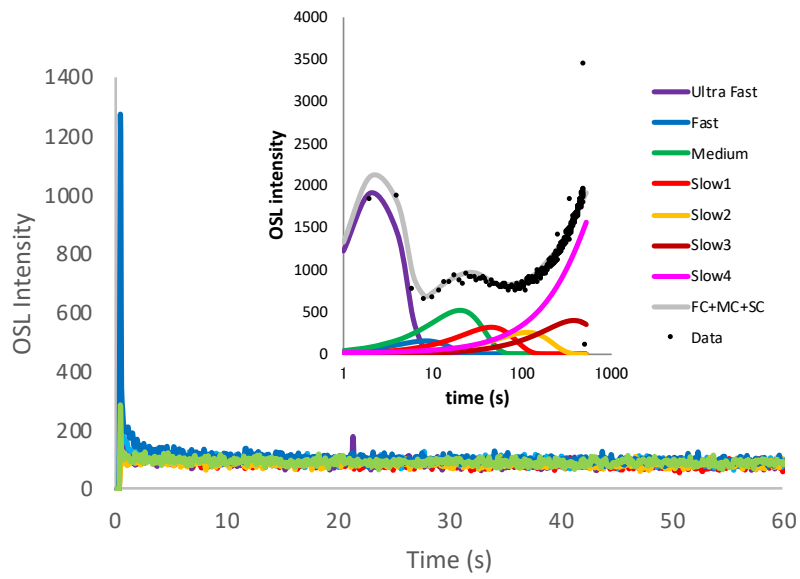
Figure 4-17. Examples of NFD1 966 OSL and LM-OSL measurements.
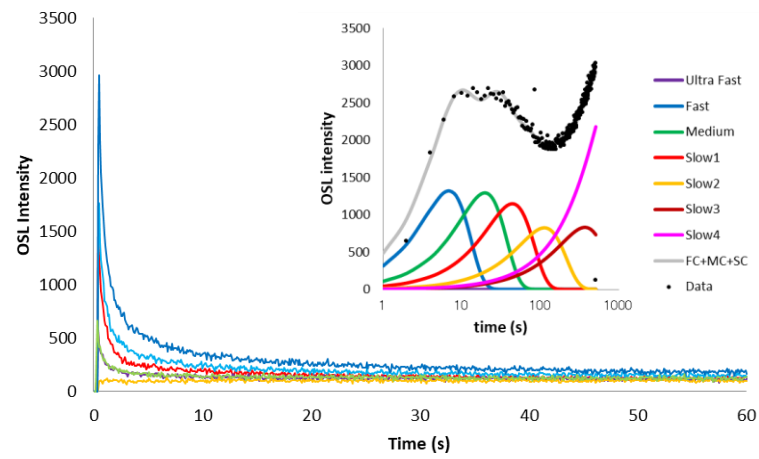
Figure 4-18. Examples of NFD1 S4 OSL and LM-OSL measurements.
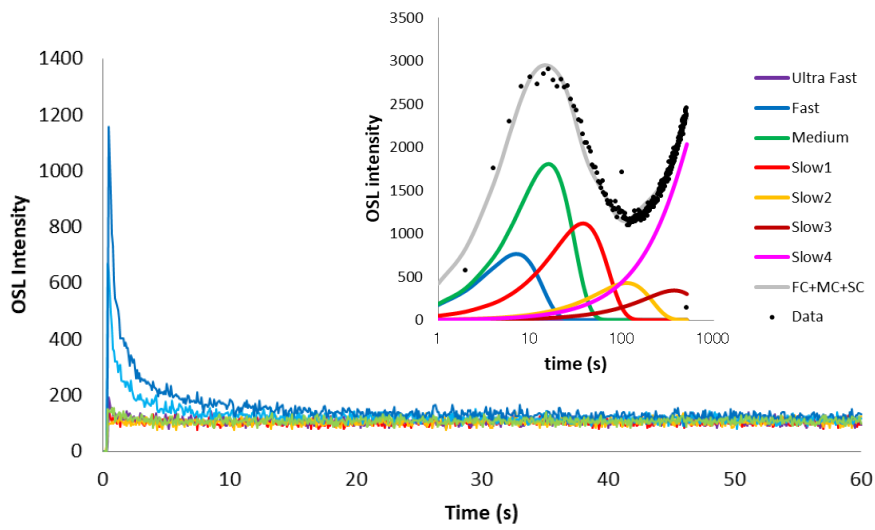
Figure 4-19. Examples of NFD1 S2 OSL and LM-OSL measurements.

Table 4-1. Assessing the impact of light sources by equivalent doses (De)

Light source	Equivalent dose (De)	Decay ratio (%)
LED	4.57±0.19 Gy	3
Toshiba	2.69±0.61 Gy	43
Photo	4.77±0.49 Gy	0

Table 4-2. Accumulated dose calculated by TL and OSL of the AFD2 core

		TL		OSL
AFD2 fa-1 118.58	site 2	262.0 ±	73.9	-
	site 3	184.4 ±	77.3	
AFD2 fa-1 118.60	site 2	260.0 ±	98.0	-
	site 3	135.3 ±	48.6	
AFD2 fa-1 white	site 2	330.6 ±	68.9	-
	site 3	135.5 ±	34.0	
AFD2 fa-5 5-1	site 2	411.4		105.0
	site 3	360.2		
AFD2 fa-5 5-2	site 2	369.6		82.2
	site 3	330.4		
AFD2 fa-5 5-3	site 2	661.3		34.6
	site 3	546.8		
AFD2 fa-5 5-4	site 2	648.0		51.1
	site 3	437.6		

Table 4-3. Accumulated dose measurements by OSL of basement rocks. The data for the ash-covered Sample with Ultrafast UF component

		De (Gy)	Average dose (Gy)	Average dose eith Uf (Gy)	Average De without Uf (Gy)
TS	1	34.80	16.90 ± 16.43	28.97 ± 10.13	4.82 ± 1.43
	2	34.84			
	3	6.37			
	4	17.28			
	5	3.54			
	6	4.54			
NFD1 800	1	2.30	8.46 ± 9.88	14.33 ± 11.81	2.58 ± 0.87
	2	9.00			
	3	27.87			
	4	3.57			
	5	6.13			
	6	1.89			
NFD1 966	1	8.90	6.64 ± 2.34	6.64 ± 2.34	— ± —
	2	6.72			
	3	7.98			
	4	3.88			
	5	8.69			
	6	3.70			

Table 4-4. Accumulated dose from OSL measurements of NFD2

		De (Gy)	Average De (Gy)		
NFD-2	1	4.05	8.28	±	5.99
		12.52			
	2A	3.15	4.90	±	2.47
		6.64			
	2B	0.78	1.11	±	0.46
		1.43			
	3	1.60	1.32	±	0.40
		1.04			

Table 4-5. OSL measurement results for NFD1-S4. Thin lines indicate half-split core boundaries; coloured samples are samples collected from the gouge.

	De (Gy)
1	39.90
2	44.40
3	42.50
4	67.30
5	49.80
6	22.00
7	29.40
8	23.70
9	24.20
10	22.90
11	24.20
12	25.00

Table 4-6. Accumulated dose from OSL measurements of NFD1-S2. Measurement results. Ash-covered data are samples with Ultrafast (UF) component.

	De (Gy)	Average De (Gy)
1	0.42	0.37 ± 0.08
	0.31	
2	0.92	1.36 ± 0.63
	1.81	
3	0.35	0.29 ± 0.08
	0.34	

Table 4-7. Trace element analysis concentration results and annual doses.

	Altitute (m)	K_2O (%)	Rb (ppm)	SE (ppm)	Th (ppm)	SE (ppm)	U (ppm)	SE (ppm)	water content	AD (Gy/kyr)
TS	5	4.2	391.5	9.2	45.1	20.6	8.9	0.2	0.0	9.7
E1	–	4.3	297.4	22.1	11.9	1.6	2.9	0.6	0.0	5.4
S5	–	5.0	226.9	22.8	88.7	11.3	15.4	3.9	0.0	15.0
S7	–	4.4	189.2	15.8	27.6	3.2	3.3	0.6	0.0	6.7
NFD1S4 (605.25 – 605.65m)	–	3.5	187.0	9.0	8.5	0.7	7.2	0.4	0.0	5.4

Table 4-8. Accumulated dose and age values by OSL method for NFD1 S2.

		De (Gy)	Average De (Gy)	Age (a)*	Age (a)**
NFD1 S2 1	1	0.29	0.22	26	41
	2	0.15			
NFD1 S2 2	1	1.01	1.41	166	261
	2	1.81			
NFD1 S2 3	1	0.35	0.49	57	90
	2	0.63			

* The average annual dose is used to calculate the age value.

** NFD1 S4 annual doses are used to calculate age values.

Table 4-9. Accumulated dose measurement results from OSL measurements of
NFD1 966. Ashing data for samples with Ultrafast (UF) component.

		De (Gy)	Average De (De)
NFD1 966 2	1	3.42	
	2	2.5	2.96 ± 0.65
	3	error	
NFD1 966 3	1	5.22	
	2	error	-
	3	0	
NFD1 966 4	1	3.14	
	2	37.39	24.76 ± 18.81
	3	33.75	
NFD1 966 5	1	109.42	
	2	22.17	53.06 ± 48.89
	3	27.59	

4.6 Reference

Ganzawa Y. Takahashi C. Miura K. and Shimizu S. (2013) Dating of active fault gouge using optical stimulated luminescence and thermoluminescence, The Journal of the Geological Society of Japan, 119, 714-726

Wintle A.G. and Murray A.S. (2006) A review of quartz optically stimulated luminescence characteristics and their relevance in single-aliquot regeneration dating protocols, Radiation Measurements, 41, 369-391

CHAPTER 5

5. General conclusions

5.1 Findings from this study

The examination of luminescence-emitting temperatures revealed that quartz separated from granite has four luminescence sites (roughly the peak temperatures of 200°C, 270°C, 340°C, and 400°C under a heating rate of 1°C/s). The lifetime of each luminescence site was then estimated. Accumulated doses and ages were determined for each luminescence site.

Two basement samples showed concordant ages of 40 ka at 270°C and 340°C emissions and more than 80 ka at a 400°C emission. These ages may be representative of the uplifting process of the basement granite. Two samples collected near the fault showed young ages compared with those of the other samples, but they were not consistent with the time of the last fault activity (about 30 years ago) partly because TL is not capable of dating modern events. The other trench samples showed various ages at 270°C and 340°C emissions different from that of the basement granite, indicating that the fault activity had some effects on the signal.

In the frictional experiments, we used quartz sand with a particle size of <150 μm and equivalent dose of 31.5 ± 16.6 Gy. Friction experiments were conducted with a rotary-shear, high-velocity friction apparatus at slip rates (V) of 200 μm s^{-1} to 1.3 m s^{-1}, normal stress of 1.0 MPa, and displacement of 10 m.

In the experiments conducted under dry conditions, the OSL signal starts to decrease from $V = 0.25$ m s^{-1} and becomes near zero at $V \geq 0.65$ m s^{-1}. OSL signal resetting is also observed in the experiment sheared at 1.3 m s^{-1} under water-added conditions. At $V = 0.25$ and 0.40 m s^{-1}, partial resetting occurs, which is characterized by coexistence of particles with and without an OSL signal.

OSL signal intensity shows a strong correlation with applied power density and frictional heat during high-velocity friction, and the signal exponentially decreases with increasing power density and temperature. The power density required for partial and complete OSL signal resetting is ~0.17 and 0.6 MW m^{-2}, respectively. Assuming a co-seismic fault slip rate of 0.6 m s^{-1}, the depths required for partial and complete resetting are expected to be ≥ 11 and ≥ 42 m.

The luminescence measurement of core samples drilled through the fault plate also demonstrated the difficulty in calculation of the exact timing of the last activity. One possible reason for this is that if the gouge had already developed, the energy to reset the luminescence signal to zero would escape as the gouge deformed without temperature rise when the fault became active. However, it was found that luminescence measurements of samples in the vicinity of the gouge can be used to calculate an age close to zero-reset. It was also found that the influence of geothermal energy needs to be taken into account, and that it is important to compare the accumulated dose against the underlying rocks, which are quite far away from the fault. These findings suggests that it may be possible to identify the most recent active part of an active fault when appropriate samples can be obtained.

The OSL measurements of the core samples focused on the ultrafast component. The results suggest that the ultrafast component may have been produced by the fracturing of quartz due to faulting activity. And since this component is highly unstable, it could be reset by heat generation during faulting. Based on the results, it is concluded that NFD2 is most likely to be the active fault section that was active in 1995.

In addition, faults of historical age, errors of around 100 years are not considered to be of any concern, and samples from a depth of around 300 m may be sufficient for evaluation. However, this is not the case for older faults, where a strike-slip rise of more than 300 m is expected. A reset of the age value could not be detected even in the sample from the Asano fault (200 m depth), but this could be because the depth of the sample was not sufficient, there may have been a problem in the identification of the fault, and in addition, it is possible that the sample was not detected because of the emphasis on the analysis of the gouge. In the future, it may be necessary to tighten the evaluation of geothermal effects (collecting information shallower than 800 m), to verify the hypothesis at the Nojima fault by analysing samples close to the gouge at the Asano fault, and to evaluate the degree of resetting of age values at each depth.

5.2 sample requrement for fault dating

1. Measuring samples of base rock in the gouge nearest neighbour provides a minimum accumulated dose. Analysis and comparison of the most recently affected layers from the faulted clay, and samples not affected by the fault, is essential.

2. In TL and OSL measurements, the signal components must always be separated and accumulated doses should be estimated for each component. Analysis of the signal in the TL lower temperature section and the ultra fast component of the OSL are potentially the key.

3. Surface samples are not suitable for thermal effects, however, samples that are too deep are also unsuitable because of geothermal effects (For the Nojima fault, a depth of 42 to 700 m is suitable.).

4. In samples extracted from deep cores, the outer part of the core cannot be used for dating due to heat generated during excavation. Signal analysis on fewer samples obtained from the centre of the core is essential.

5. Single grain dating is preferred, as fault active surfaces contain samples of various elementary characteristics. However, it is currently difficult to observe the weak signal of single particles.